Superconducting bearings for flywheel applications

Abrahamsen, Asger Bech

Publication date:
2001

Document Version
Publisher's PDF, also known as Version of record

Risø–R–1265(EN)

Superconducting bearings for flywheel applications

Asger Bech Abrahamsen

Risø National Laboratory, Roskilde, Denmark
May 2001

Abstract A literature study on the application of superconducting bearings in energy storage flywheel systems. The physics of magnetic levitation and superconductors are presented in the first parts of the report, followed by a discussion of the literature found on the applications of superconducting bearings in flywheels.

ISBN 87–550–2877–2(internet)
ISSN 0106–2840

Print: Danka Services International A/S · 2001

Contents

1 Introduction

Flywheels are typically used as local energy storage for application where a short and large power consumption exceeds the available power supplied by the electrical distribution network. However increasing introduction of example windmills into the power network have increased the demand for a long term energy storage, where power produced during the night can be stored for the next morning when the consumers want their coffee. The friction losses in traditional flywheels have been to large to efficiently store energy for the 12 hour consumer period, but the development of magnetic and superconducting bearings have reduced the friction losses by several orders of magnitude and flywheel designs have been reconsidered during the last decade.

This report summarizes a literature study done in 1999 on the application of high temperature superconductors for bearings in flywheels used for energy storage. The aim of the report is to outline the basic concepts of magnetic and superconducting levitation to people who are not familiar with magnetic forces and the physics of superconductors, and to present an overview of the current status of the research field.

The report consist of a short introduction to the basic properties of conventional bearings and then a calculation of the friction loss limit expected for a flywheel constructed at Risø. It is shown that conventional bearings can not fulfill the friction loss limit whereby a new bearing technology such as magnetic or superconducting levitation is needed. An introduction to magnetic levitation and superconductivity is given in order to evaluate the basic bearing properties of superconducting bearings. The last section shows examples of operating superconducting flywheel systems found in the literature.

Asger Bech Abrahamsen
Materials Research Department, Risø

2 Basic concepts of bearings

The invention of the bearing is directly linked to the invention of the wheel approximately 3000 BC in ancient Iraq where a wood plate was mounted onto a wood shaft. Later in history the concept of shafts and bearings was the main technology of the industrial revolution in the 1700 century. Today bearings are used in almost all machinery made by man kind, including flywheels.

2.1 Key parameters

A bearing for a flywheel system have the following parameters of interest to the designer.

- Static load capacity in terms of lifting force.
- Stiffness
- Coefficient of friction
- Non-linearity of lifting forces and dynamic stability.

Static load capacity

Standard bearings are constructed of an outer house and an inner rotating part mounted on the shaft which is to be supported. The contact between the inner and outer part is conducted by rolling objects or by a fluid film such as oil. Thus the static load capacity is determined by the onset of plastic deformation of the rolling objects or by the removal of the fluid film between the moving parts.

Stiffness

The stiffness κ of a bearing is defined as the derivative of the bearing force with respect to a small displacement of the shaft away from equilibrium.

$$\kappa = - \left. \frac{dF}{dx} \right|_{\mathrm{x} = x_0} \tag{1}$$

Thus the stiffness describes the linear force response of the bearing. In the mechanical or fluid bearing the stiffness is determined by the elasticity of the rolling objects or the compressibility of the fluid.

Coefficient of friction

The coefficient of friction is a measure of the drag force on the moving parts of the bearing. It is defined as the ratio between the drag force F_D and the lifting force F_L of the bearing.

$$\mu = \frac{F_D}{F_L} \tag{2}$$

This definition is equivalent to the drag force on a solid body which is moved on a surface. The lifting force is then given by the force of gravity on the solid body.

Non-linearity and dynamic stability

The equation of motion of a shaft rotating in a bearing will depend on the stiffness in a linear response theory, but the relation between lifting force and displacement will often be non-linear. Thus in a more realistic treatment of the system one must operate with non-linear equations of motion. This will cause system dynamics, which is much more complicated than predicted from linear response theory and even chaotic motion can arise.

3 Flywheel design

A flywheel is a device for storing kinetic energy in the form of rotational motion of a wheel on a shaft. The kinetic energy is related to the rotation speed ω and the moment of inertia of the flywheel I

$$E_{kin} = \frac{1}{2} I\omega^2 \tag{3}$$

3.1 Friction losses

In order to compare the friction losses of different bearings used in superconducting flywheel systems J.R. Hull et al. [1] introduced a coefficient of friction defined by equation (2). Figure 1 shows a simple flywheel of mass M and radius R with a vertical rotation axis supported by ball bearings. The drag force F_D of the bearings causes a torque on the rotation axis of radius R_D

$$|\tau| = |\mathbf{R_D} \times \mathbf{F_D}| = -I\frac{d\omega}{dt} \tag{4}$$

where I is the moment of inertia of the flywheel. By inserting $I = MR^2$ and the lifting force equal to the force of gravity $F_L = Mg$ one gets a coefficient of friction given by

$$\mu = -\frac{R^2}{gR_D}\frac{d\omega}{dt} \tag{5}$$

Thus the coefficient of friction causes a decrease of the flywheel rotation velocity in time and it depends on the specific geometry of the flywheel system. One can insert the angular acceleration determined from the kinetic energy given by equation (3) and obtain an expression for the relative energy loss of the system

$$\frac{\frac{dE}{dt}}{E} = -\frac{2gR_D}{R^2}\frac{\mu}{\omega} \tag{6}$$

which shows that in order to decrease the relative energy loss one must either reduce the coefficient of friction or speed up the flywheel. The dependence of ω reflects that the drag losses scale with ω whereas the kinetic energy scales with ω^2. It has been assumed that the drag force is independent of the flywheel velocity in the derivation above.

3.2 Coefficient of friction of Risø flywheel

The Materials Research Department at Risø have constructed a prototype flywheel for storage of 1 kWh = 3.6 MJ. This is obtained by spinning a rotor with radius R = 0.2 m and a weight of M = 20 kg at 30000 RPM ($\omega_0 = 3.2 \cdot 10^3\ rad\ s^{-1}$. By integrating equation (5) one can determine the fraction of the initial kinetic energy which is present at a given time :

$$\frac{E}{E_0} = \frac{\frac{1}{2}I\omega^2}{\frac{1}{2}I\omega_0^2} = (1 - \frac{\mu g R_D}{\omega_0 R^2}t)^2 \tag{7}$$

whereby one can estimate the limit of μ if the flywheel must run for 12 hours before 10 percent of the energy has been lost given $R_D = 0.01$ m and $g = 9.82$ m s^{-2}

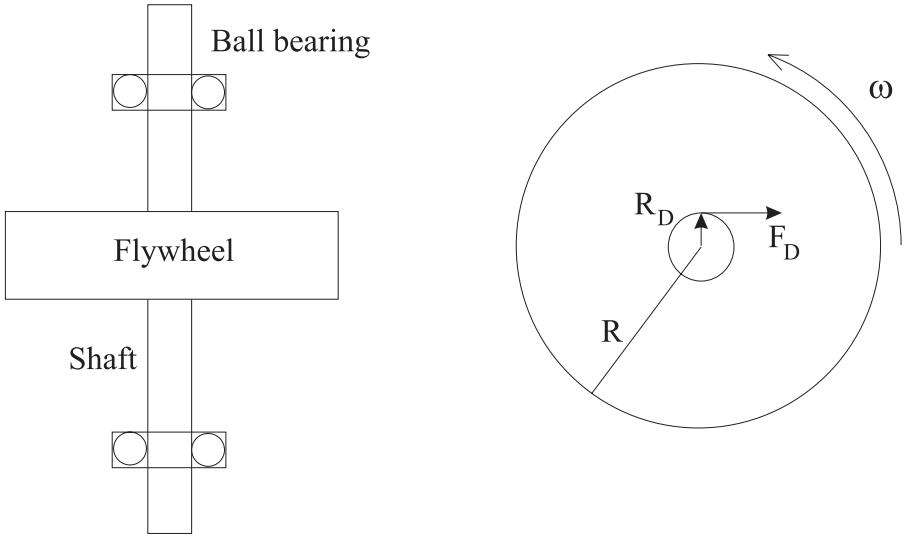

Figure 1. Left: Flywheel system supported by ball bearings. Right: Flywheel disk of radius R seen from the top. The drag force of the ball bearings is indicated by F_D and is acting on the shaft of radius R_D.

$$\mu = \frac{\omega_0 R^2}{g R_D t_{\frac{E}{E_0}}}(1 - \sqrt{\frac{E}{E_0}}) = 1.5 \cdot 10^{-3} \tag{8}$$

Ordinary ball bearings typically have a $\mu = 10^{-3}$, but the calculation above is only for the kinetic energy loss and if there are additional losses in motor/generator or power converters one must operate with a lower limit of the bearing friction in order to fulfill the 10 percent total energy loss during 12 hours. If this result in a 1 percent kinetic energy loss limit during 12 hours one obtain a limit of $\mu = 10^{-4}$ whereby ball bearings are insufficient.

The main problem with conventional bearings is the mechanical contact between the shaft and the bearing mounting house, which causes the high coefficient of friction and wear of the bearings resulting in a demand for maintenance. In order to improve the performance of the bearing one would like to keep the shaft positioned in space without touching it. This can be done using magnetic forces created by permanent magnets or electromagnets.

The following sections will introduce concepts of magnetic forces and show that some stabilizing element is needed in the application of magnetic bearings.

4 Magnetic levitation

Everybody have tried to play with two magnets and experienced the repulsion when poles of the same kind are facing each other. One often speculates that it would be nice to use this repulsion to balance gravity and thereby have a magnet levitated without any mechanical contact.

In 1842 Earnshaw proved that the above can not be done for a static system of permanent magnets. This will be illustrated and the potential of magnetic levitation will be discussed in this chapter.

4.1 Earnshaw's theorem

The consequence of Earnshaw's theorem [2] is that permanent magnets can only be in a saddle point equilibrium where two directions are stable and the last direction is unstable. This can be illustrated by considering a permanent magnet with the north pole facing a north pole of a large fixed magnet as shown in figure 2.

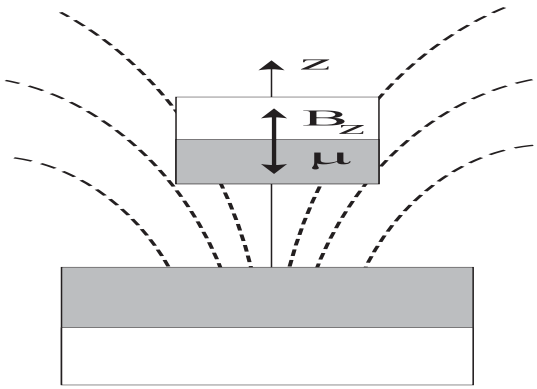

Figure 2. Illustration of Earnshaws theorem by two magnets with equal poles facing each other. μ denotes the dipole moment of the magnet levitated a distance z above the lower magnet, which creates a field B_z at the position of the top magnet. The field lines of the lower magnet are indicated by dash lines.

By assuming the magnets are rotational symmetric with respect to the z-axis and that the top magnet can be considered as a point at the center of mass one can write the energy of the upper magnet as the sum of a gravity term and a dipole interaction term

$$U = mgz - \boldsymbol{\mu} \cdot \mathbf{B} = mgz - \mu B_z cos(\theta) \tag{9}$$

where m is the mass of the magnet levitated a distance z, g is the acceleration of gravity, $\boldsymbol{\mu}$ is the dipole moment of the magnet and B_z is the magnetic field created by the lower magnet at position z and θ is the angle between the field and the dipole direction.

The equilibrium of the top magnet is determined by a vanishing derivative of U with respect to the three coordinates and the tilt angle θ of the magnet.

$$\frac{\partial U}{\partial r_i} = 0 \quad \text{for} \quad r_i = x, y, z, \theta \tag{10}$$

By evaluating the above on (9) at $x = y = 0$, $z = z_0$ and $\theta = 180^o$ one gets

$$\frac{\partial U}{\partial x} = \mu \frac{\partial B_z}{\partial x} = 0 \tag{11}$$

$$\frac{\partial U}{\partial y} = \mu \frac{\partial B_z}{\partial y} = 0 \tag{12}$$

$$\frac{\partial U}{\partial z} = mg + \mu \frac{\partial B_z}{\partial z} = 0 \tag{13}$$

$$\frac{\partial U}{\partial \theta} = \mu B_z sin(\theta) = 0 \tag{14}$$

The two first equations are fulfilled because the z-component of the magnetic field is maximum at the symmetry axis given a derivative of zero. From the third equation it is seen that the magnetic levitation force is caused by the decreasing field strength as one gets further away from the bottom magnet. The fourth equation gives zero because $sin(180^o) = 0$.

Now for the equilibrium to be stable one must demand that the system is in an energy minimum whereby the second derivative of the energy U must be positive with respect to all directions in space and the tilt angle

$$\frac{\partial^2 U}{\partial r_i^2} = \mu \frac{\partial^2 B_z}{\partial r_i^2} > 0 \quad \text{for} \quad r_i = x, y, z \tag{15}$$

$$\frac{\partial^2 U}{\partial \theta^2} = \mu B_z > 0 \tag{16}$$

The spatial condition is examined using Maxwell's fundamental equations of electromagnetism. Since there are no currents running in the system it is concluded that the rotation of the magnetic flux density $\mathbf{B}$ is zero and $\mathbf{B}$ is therefore determined by the Laplace law

$$\begin{cases} \nabla \cdot \mathbf{B} = 0 \\ \nabla \times \mathbf{B} = \mathbf{J} = 0 \end{cases} \Rightarrow \nabla^2 \mathbf{B} = 0 \tag{17}$$

which gives the following conditions for the second derivatives of the B_z component

$$\frac{d^2 B_z}{dx^2} + \frac{d^2 B_z}{dy^2} + \frac{d^2 B_z}{dz^2} = 0 \tag{18}$$

Thus it is impossible to have positive second derivatives in both the x, y and z direction at the same time which show that the stable equilibrium condition (15) can not be fulfilled for all tree coordinates. This is also what is found when (15) is evaluated on equation (11). The second derivative with respect to the z-axis is positive because the magnetic field from the lower magnet decays like r^{-3}, but the negative second derivatives with respect to x and y are obtained because the z components of the magnetic field attains a maximum at the symmetry axis.

The second derivative of the energy with respect to the tilt angle is negative $\frac{\partial^2 U}{\partial \theta^2} = \mu B_z cos(180^o) < 0$ showing that the system is unstable with respect to tilts. Thus the magnet on figure (2) will flip and be attracted to the north pole of the lower magnet by an infinitely small disturbance.

Earnshaw's theorem generally states that any collection of magnetic particles which must fulfill the Laplace equation given in (17) can not be in a stable equilibrium in all directions. What is learned from Earnshaws theorem is that it is not just a question of finding a sufficient cleaver configuration of permanent magnets in order to obtain stable equilibrium. Some other component than permanent magnets must be added to the system.

4.2 Magnetic forces

Magnetic fields are generated by moving charged particles or by the ordering of the particle spins in solids. The magnetic flux density $\mathbf{B}$ is given by the sum of the free space magnetic field strength $\mathbf{H}$ and the magnetization density $\mathbf{M}$ caused by the ordering of the moments of the atoms in a solid

$$\mathbf{B} = \mu_0(\mathbf{H} + \mathbf{M}) \tag{19}$$

where μ_0 is the vacuum permeability.

In order to calculate the forces between a magnetic field and a magnetized solid body one often consider the moment of the atoms in the solid as generated by small current loops. This picture is inspired by the fact that the electrons are moving around the nuclei of the atom in orbitals. In the derivation below it will be assumed that magnetic fields are only created by currents and the connection to the magnetization density will be shown.

The force on a small wire $d\mathbf{s}$ with charges q of density n moving at velocity v in a magnetic field $\mathbf{B}$ is given by the sum of the Lorenz force $\mathbf{F} = q\mathbf{E} + q\mathbf{v} \times \mathbf{B}$ acting on the electrons [3]. By assuming the electrical field to be zero ($\mathbf{E} = 0$) one gets

$$\begin{aligned} d\mathbf{F_{ds}} &= \int_{wire} nq\mathbf{v} \times \mathbf{B} d\mathbf{r} \\ &= (\int_A \mathbf{J} dA) d\mathbf{s} \times \mathbf{B} \\ &= I d\mathbf{s} \times \mathbf{B} \end{aligned} \tag{20}$$

where the current density is given by $\mathbf{J} = nq\mathbf{v}$ and the integration of the current density across the cross section A of the wire gives the total current I in the wire.

One can then calculate the force on a small loop by integrating the above equation along the loop

$$\begin{aligned} \mathbf{F_{loop}} &= \int_{loop} I d\mathbf{s} \times \mathbf{B} \\ &= -I \int_{area} (\nabla \cdot \mathbf{B}) d\mathbf{S} - I \int_{area} (\nabla \times \mathbf{B}) \times d\mathbf{S} + I \int_{area} (d\mathbf{S} \cdot \nabla) \mathbf{B} \\ &= I \int_{area} (d\mathbf{S} \cdot \nabla) \mathbf{B} \end{aligned} \tag{21}$$

using $\nabla \cdot \mathbf{B} = 0$ and $\nabla \times \mathbf{B} = \mu \mathbf{J} = 0$ since the small loop is placed in vacuum. Furthermore a vector identity [1] has been used to transform the integral from a line- to a surface integral over the loop area. Since the size of the current loop will be of the length scale of atoms it can be assumed that the gradient of the flux density B will be constant across the current loop. Thus the force on the loop is given by

$$\mathbf{F_{loop}} = (I\mathbf{S} \cdot \nabla)\mathbf{B} \tag{23}$$

which show that the properties of the current loop is given by the quantity $\mathbf{m} = I\mathbf{S}$, which is called the dipole moment of the loop. By dividing the loop force

[1] [3] page 106

$$\int_{loop} \mathbf{P} \times d\mathbf{s} = \int_{area} (\nabla \cdot \mathbf{P}) d\mathbf{S} + \int_{area} (\nabla \times \mathbf{P}) \times d\mathbf{S} - \int_{area} (d\mathbf{S} \cdot \nabla) \mathbf{P} \tag{22}$$

with the characteristic volume of the loop one can determine the force density $\rho_{\mathbf{F}}$ on the volume of the loop.

$$\rho_{\mathbf{F}}(\mathbf{r}) = (\mathbf{M} \cdot \nabla)\mathbf{B} \tag{24}$$

where the magnetization density $\mathbf{M} = \mathbf{m}/V_{loop}$ has been introduced. The magnetization density can be considered as the magnetic field created in the center of the small current loop and it is therefore possible to write the magnetic flux density given by (19) as the sum of the vacuum field strength $\mathbf{H}$ created by macroscopic currents in coils and the magnetization density $\mathbf{M}$ created by microscopic currents circulating around the atoms of a solid.

The total force on a solid containing many atomic moments can now be calculated from the force density of the equivalent current loops

$$\mathbf{F} = \int_{sample} \rho_F(\mathbf{r}) d\mathbf{r} = \int_{sample} (\mathbf{M} \cdot \nabla)\mathbf{B} d\mathbf{r} \tag{25}$$

Thus one can calculate the force on a magnetized body if the spatial magnetization density in the solid and the magnetic field distribution from all sources is known. The task of calculating field distributions in arbitrary geometries can be quite difficult and often one has to use finite element methods to solve Maxwell's equations.

4.3 Magnetic stresses

Maxwell and Faraday imagined that the forces between different magnets could be represented by the lines of magnetic forces or magnetic field lines. In their picture tension acts along the field lines and a pressure force acts normal to the field lines. It can be shown [2] that the force $d\mathbf{F}$ acting on a surface element as illustrated on figure (3) can be decomposed into forces given by the normal and tangential field components $\mathbf{B} = B_n\mathbf{n} + B_s\mathbf{s}$

$$d\mathbf{F} = [(\sigma - p_m)\mathbf{n} + \tau_m\mathbf{s}]dA \tag{26}$$

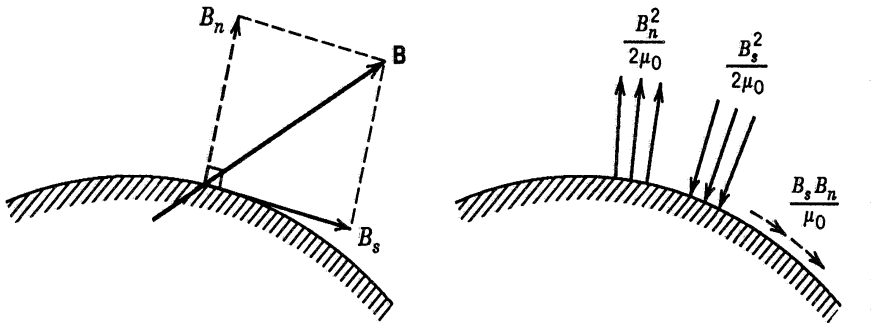

Figure 3. Left : Definition of the surface and normal component of the magnetic flux density at a surface in space. Right : The magnetic tension, pressure and shear forces on the surface caused by the surface and normal field components are shown by arrows.

[2] [4], [5]

where σ is the magnetic tension, p_m is the magnetic pressure and τ_m is the magnetic shear given by

$$\sigma = \frac{B_n^2}{2\mu_0} \tag{27}$$

$$p_m = \frac{B_s^2}{2\mu_0} \tag{28}$$

$$\tau_m = \frac{B_n B_s}{\mu_0} \tag{29}$$

One can then determine the total force on the magnetic sources in a volume V by integrating the above expression over the surface S_V defining V

$$\mathbf{F} = \frac{1}{2\mu_0} \int_{S_V} [(B_n^2 - B_s^2)\mathbf{n} + 2B_n B_n \mathbf{s}] dA \tag{30}$$

To illustrate the concept of magnetic tension figure (4) show two different magnet poles facing each other. The magnetic field lines are seen at left and since there is only a normal field component at the pole surfaces a tension will act on both magnets which is shown to the right. One can determine the total force on one of the magnets by calculating the difference in the tension at the two ends. The magnetic field around the two magnets is given by the vector sum of the fields of the two magnets, whereby the normal field components at the poles facing each other will be larger than the field components at the poles pointing away from each other. Thus the magnets will attract one another.

Figure (5) illustrate the concept of magnetic pressure between two magnetic poles of the same kind facing each other. Since the magnetic field lines must be closed curves from north to south pole($\nabla \cdot \mathbf{B} = 0$), it is seen , that only a tangential field component is present at the symmetry plane between the magnets. This result in a magnetic pressure on the two magnets and they repel each other.

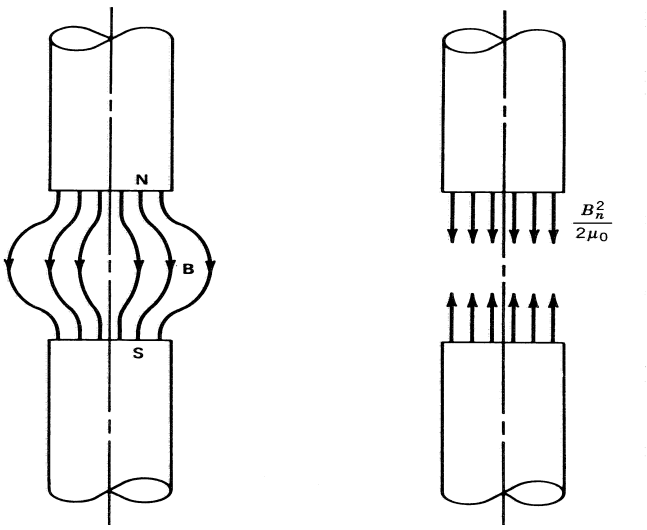

Figure 4. Left: Magnetic field lines between a north and a south pole facing each other. Right: Magnetic tension between the poles caused by the normal field component at the pole surfaces.

In order to get an estimate of the maximum force between two magnets one can calculate the magnetic tension σ or pressure p_m from 27. Permanent magnets

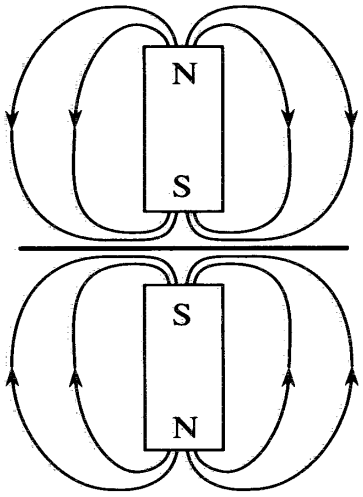

Figure 5. Magnetic field lines around two dipole magnets with identical poles facing each other. There is only a tangential field component at the symmetry plane between the magnets resulting in a magnetic pressure pushing the dipoles apart.

today can be purchased with a surface field of approximately 0.5 Tesla [6], which gives

$$\sigma = \frac{B_n^2}{2\mu_0} = \frac{(0.5 \text{ T})^2}{2 \cdot 4\pi 10^{-7} \quad \text{NA}^{-2}} = 10 \text{ Ncm}^{-2} \tag{31}$$

If it was possible to have stable levitation with permanent magnets one can estimate the surface area of magnets needed to lift a flywheel with a mass of 20 kg. The magnetic pressure is equivalent to lifting 1 kg per cm^2 and one therefore needs approximately 20 cm^2 of 0.5 Tesla magnet poles of the same kind facing each other.

4.4 Magnetic bearing

Since stable magnetic levitation can only be obtained in two directions at the same time as shown in section (4.1), one has to stabilize the last direction with a mechanical contact or with electromagnetic forces produced by some regulation electronics. Figure (6) shows a typical passive magnetic bearing where the repulsion between two equal poles is used to levitate the shaft. The shaft is however unstable with respect to tilts away from the symmetry axis of the bearing magnets and the mechanical support of the shaft prevent the tilt. Figure (7) show a typically electromechanical design where a sensor is part of a feed back loop which changes the magnetic forces of the bearing in order to maintain the same shaft position. One common application for active magnetic bearings is the support of the rotor in turbo molecular pumps for obtaining ultra high vacuum.

The major drawback of the two stabilization principles shown above is that losses are introduced by the mechanical contact or inefficient power conversion in the electronics of the control system.

Superconductors can be introduced into magnetic bearings in order to stabilize the system in all three direction, because superconductors can trap magnetic field and thereby prevent a magnet from tilting. Thus the mechanical support of the shaft shown on figure (6) can be replaced by a superconductor and a small magnet on the shaft, whereby stable levitation is obtained without any contact between

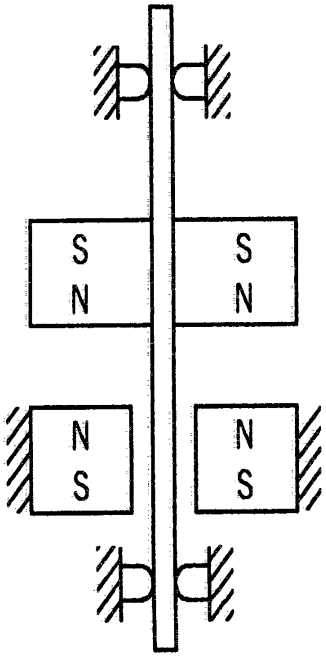

Figure 6. Passive magnetic bearing with mechanical support of shaft, because the system is unstable with respect to tilts away from the rotation axis.

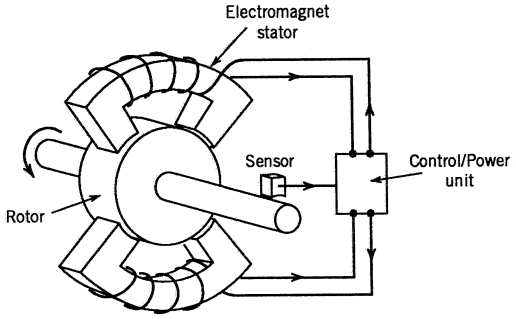

Figure 7. Active magnetic bearing with a feedback loop controlling the bearing position along the unstable direction of the system.

shaft and the surroundings. This is discussed in details in the following chapters.

5 Superconductivity

Superconductors can be used to obtain intrinsically stable levitation of a permanent magnet, because the magnetic field of the magnet can be trapped in the superconductor due to a phenomena called flux pinning. Basic superconductor properties will be introduced in this chapter in order to explain the concepts of flux pinning and to discuss the levitation potential of superconductors.

5.1 Cooper pairs

Conventional superconductivity is caused by pairing of two conduction electrons with opposite wave vector and spin by the creation of oscillations in the position of the ions in the crystal lattice of the superconductor. The paired electrons are called Cooper pairs.

A fundamental puzzling question of superconductivity is how the Cooper pairs consisting of electrons which normally repel each other are created. A qualitative explanation is illustrated on figure (8), which shows how the movement of an electron in a lattice of positive ions can cause a lattice contraction due to the attraction between the negative electron and the positive ions. The delay in the movement of the ions compared to the position of the electron is due to the large mass difference between the electron and the ions. A local increased density of positive charge result from the lattice contraction and another electron will be attracted to this region. Thus the two electrons are paired by the creation of a lattice oscillation and the pairing mechanism is often referred to as the phonon mediated interaction, since lattice oscillations exited at finite temperature are called phonons. The lattice oscillations exited by the moving electrons are often called virtual phonons. The two electrons in the Cooper pair will however not stay together for long time since they are moving away from each other. When the separation gets too large the Cooper pair changes partner with another Cooper pair whereby the distance between the electrons remains limited in the pair.

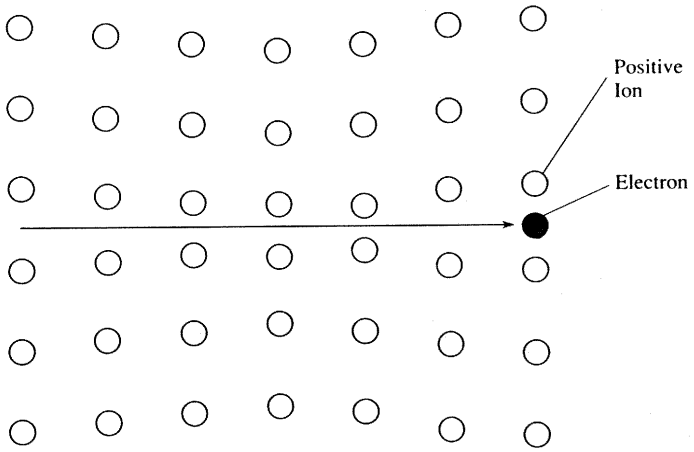

Figure 8. Illustration of the excitation of a lattice oscillation, caused by the movement of a negative charged electron in a lattice of positive charged ions, resulting in paring of electrons into Cooper pairs in a superconductor.

Superconductivity only exists below a characteristic critical temperature T_c, where the thermal fluctuations are sufficient small compared to the phonon-mediated attraction between the electrons. As the temperature is lowered below the critical

temperature T_c there will be two kinds of electrons present in the superconductor. Some normal electrons and some electrons which have been paired into Cooper pairs. The total number of electrons in a superconductor will be constant, but more and more normal electrons will be paired into Cooper pairs as the temperature is lowered below the critical temperature. This view on superconductivity is called the Gorter-Casimir two-fluid model [7, 8].

In order to break a Cooper pair one must add an energy equivalent to the binding energy of the pair. The state of a superconductor or a region in a superconductor only containing normal electrons is called the normal state.

5.2 Critical current density

One fundamental property of the superconducting state is the ability to conduct a current without any loss, which is the origin of the name superconductor. A qualitative explanation for this property is that a transport current in a superconductor will cause a net flow of all electrons in the superconductor, and if one electron in a Cooper pair is scattered by an impurity this electron will just change partner, but remain in the superconducting state if the energy exchange in the scattering process is lower than the Cooper pair binding energy. Thus the transport of Cooper pairs is not sensitive to impurities as transport of electrons is in a normal conductor at low temperatures. There is a upper critical current density J_c which can be sent through the superconductor, because the Cooper pairs are broken when the kinetic energy difference between the two electrons in the Cooper pair due to the current exceeds the binding energy of the Cooper pair.

Meissner effect

A Cooper pair consist of two electrons with opposite spin and wave vector $(-k\uparrow, k\downarrow)$. All the Cooper pairs in a superconductor are correlated and can be described by a macroscopic wave function Ψ. By considering the superfluid as a molecule it is seen that the momentum is zero, $\mathbf{p} = -\hbar\mathbf{k} + \hbar\mathbf{k} = 0$. In the presence of a magnetic field the momentum is changed by the vector potential and supercurrents will begin to flow due to momentum conservation :

$$\mathbf{P} = \mathbf{p} + q^*\mathbf{A} = 0 \qquad \Rightarrow \tag{32}$$

$$\mathbf{j} = -\frac{nq^{*2}}{m^*}\mathbf{A} \tag{33}$$

where $\mathbf{P}$ is the canonical momentum, $\mathbf{p}$ is the momentum when no magnetic field is present ($\mathbf{p} = m^*\mathbf{v}$) and $\mathbf{A}$ is the vector potential, $\nabla \times \mathbf{A} = \mathbf{B}$. The Cooper pair velocity has been related to the current density, $\mathbf{j} = nq^*\mathbf{v}$.

The result of equation (33) is that supercurrents will run in the opposite direction of the vector potential. This causes a circulating supercurrent at the edge of the sample whereby the applied field is removed from the interior of the sample when it becomes superconducting. This effect is called the Meissner effect and is illutrated on figure (9).

There is a upper limit of the external magnetic field, which can be removed by the Meissner effect since the circulating supercurrent at the sample edge is limited by the critical current density J_C. Superconductivity breaks down when J_C is exceeded and the equivalent applied field is denoted the critical field H_C.

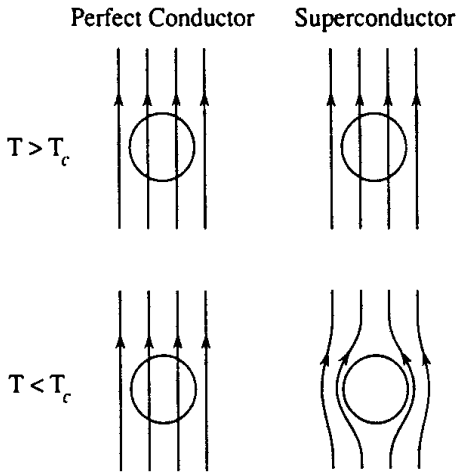

Figure 9. The magnetic field lines in a superconductor are expelled as the superconducting state is entered, because supercurrents will start to circulate at the sample edge and effectively screen out the applied magnetic field whereby $\mathbf{B} \equiv 0$ *inside the superconductor. This is known as the Meissner effect.*

5.3 Type II superconductors

Superconductors can be divided into two types depending on the ratio between the coherence length ξ and the penetration depth λ of the superconductor. The coherence length is a characteristic length scale for changes in the density of Cooper pairs and the penetration depth is a characteristic length scale for penetration of magnetic fields into a superconductor. It can be shown that the energy associated with the wall between a superconducting and a normal conducting volume will change from positive to negative when

$$\kappa = \frac{\lambda}{\xi} \tag{34}$$

becomes larger than $\frac{1}{\sqrt{2}}$. Superconductors with positive respectively negative domain wall energy are called type-I and type-II superconductors.

The consequence of the negative domain wall energy is that it is energetically favorable for a type-II superconductor to include the magnetic field lines of an applied field into the bulk in small non-superconducting regions instead of screening out the applied field. Since the superconductor gains energy by creating walls it will create as many walls as possible and include the applied field in a lot of small normal regions instead of one big. The size of the normal regions have a lower limit, which is determined by the quantum mechanical nature of the superconducting state. All the electrons in the superconducting state are described by the same macroscopic quantum mechanical wave function, which must be continuous around any closed contour. This means that the phase of the wave function must change by an integer number times 2π around the contour. It can be shown [9] that this leads to a quantization of the magnetic flux in a normal region inside of the superconductor and the quantum of the flux is called a flux quantum Φ_0 given by

$$\Phi_0 = \frac{h}{2e} \tag{35}$$

Thus when magnetic flux enters the interior of the superconductor the magnetic flux lines will be packed into small normal regions each carrying one fluxquanta. Such a normal region containing one flux quantum is called a flux line or a vortex. From Ginzburg-Landau theory [3] one can calculate how the Cooper pairs are suppressed at the center of the flux line and how the superconducting screening currents are keeping the flux in the center of the flux line, as shown on figure (10).

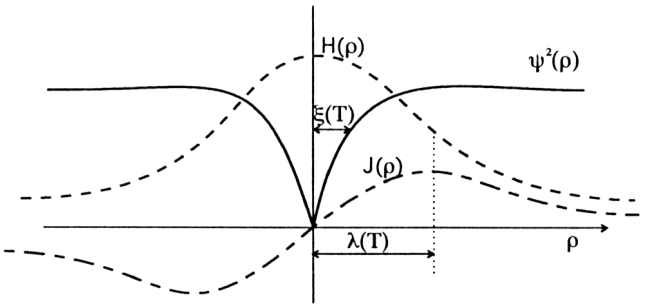

Figure 10. A flux line in a superconductor consist of a normal core where the magnetic field $H(\rho)$ is generated by supercurrents $J(\rho)$ circulating around the core. The decay of the magnetic field is determined by the penetration depth $\lambda(T)$ and the total magnetic flux associated with a flux line found by integrating the magnetic flux density $H(\rho)$ is one flux quantum Φ_0. $\psi^2(\rho)$ denotes the Cooper pair density and the size of the normal core is determined by the coherence length $\xi(T)$.

Flux lines repel one another and form a hexagonal lattice, called the flux line lattice, due to the rotational symmetry of the flux lines. This lattice can be visualized by evaporating some ferro-magnetic particles onto the surface of a superconductor when it is placed in a magnetic field. The magnetic particles will gather at the center of the flux lines because the local magnetic flux density $H(\rho)$, as shown on figure (10), is higher than far from the core of the flux line. Figure (11) shows an electron microscopy picture of a $TmNi_2B_2C$ superconductor where iron particles have been evaporated onto the surface. The white spots are piles of iron particles at the flux line cores and the hexagonal structure of the flux line lattice is easily seen.

The separation of the flux lines in the lattice is directly related to the applied magnetic field since the triangular unit cell of the lattice have $\frac{1}{6}$ of a flux quantum at each corner as shown on figure (12). The integrated flux density in the unit cell must match the number of flux quanta in the cell. By simplifying the integration to the product of the average flux density B_a and the unit cell area A_{cell} one get

$$\begin{aligned} \frac{3}{6}\Phi_0 &= B_a A_{cell} \quad \Rightarrow \\ a &= \sqrt{\frac{2\Phi_0}{\sqrt{3}B_a}} \end{aligned} \tag{36}$$

where the unit cell area as determined from figure (12) has been inserted.

The magnetic properties of a type-II superconductor are summarized in a H-T phase diagram in figure (13). At low field it is energetically favorable to expel the flux of the superconductor and make the wall to the normal phase at the edge of the sample, but at a sufficiently high field denoted H_{c1} flux lines will penetrate

[3] [9],[10]

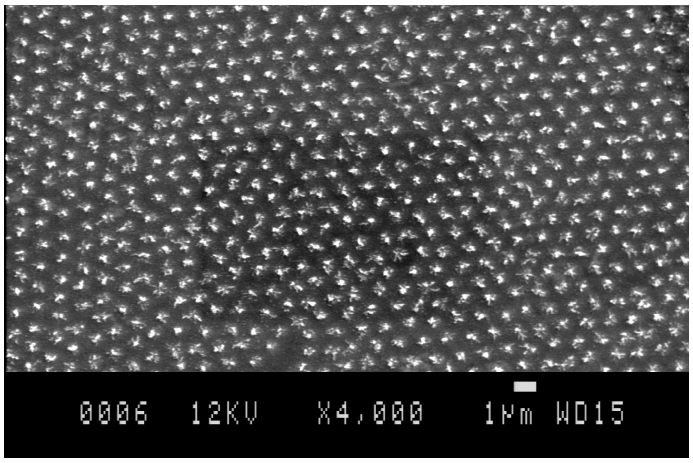

Figure 11. Electron microscopy picture of a $TmNi_2B_2C$ superconductor after ferromagnetic iron particles has been evaporated onto the surface at $T = 4.2$ K and in an applied field of $H = 20$ Oe. The white spots are piles of iron particles gathered at the cores of the flux lines due to the higher local flux density at the center of the flux lines. One can easily identify the hexagonal structure of the flux line lattice from the picture [11].

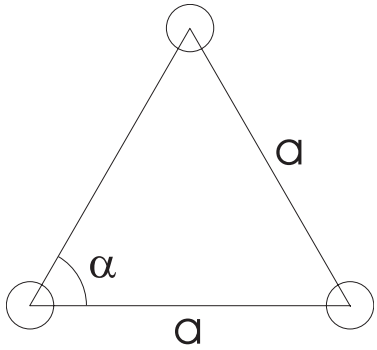

Figure 12. Unit cell of the hexagonal flux line lattice. There is one flux quantum at each lattice point giving $\frac{3}{6} = \frac{1}{2}$ flux quantum inside the hexagonal unit cell. The area of the unit cell is simply given by $A_{cell} = \frac{1}{2}a^2 sin(60^o) = \frac{\sqrt{3}}{4}a^2$ where a is the distance between the flux lines.

into the bulk of the superconductor, which will enter the mixed state as shown on figure (11). Superconductivity is suppressed when the cores of the flux lines start to overlap at a field denoted H_{c2} and the normal state of the superconductor is entered. This happens when the flux line separation a given by equation (36) becomes comparable with the size of the flux line core given by the coherence length ξ as shown on figure (10).

5.4 Flux pinning

In a clean type-II superconductor the flux lines will reversible move in and out of the sample as the applied field is changed between H_{c1} and H_{c2}, but if the superconductor contain some defects then the flux lines can be trapped at these defects. The defects result in a local reduction of the density of Cooper pairs and since there are no Cooper pairs in the flux line core it is energetically favorable

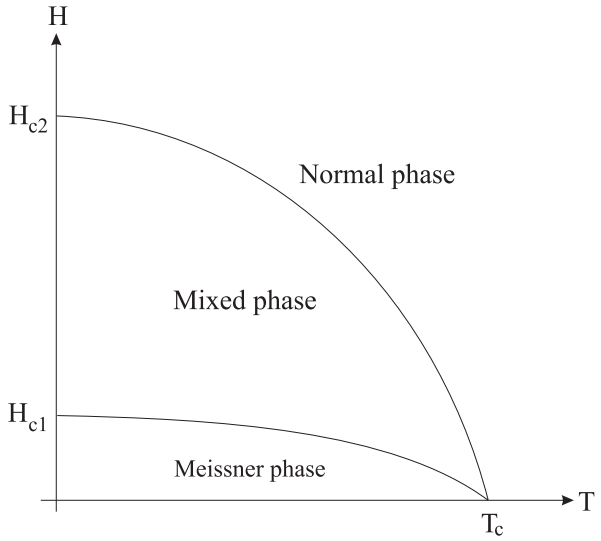

Figure 13. Phase diagram of a type-II superconductor. Below the lower critical field H_{c1} magnetic fields are expelled from the superconductor, but it becomes energetically favorable to include some of the magnetic field as flux lines above H_{c1}. Superconductivity is suppressed when the cores of the flux lines overlap at the upper critical field H_{c2}.

to place the flux line at a point where the Cooper pairs density is already low as shown on the right hand side of figure (14). The defect will appear as a potential well which is called a pinning center and a flux line trapped at a pinning center is called pinned.

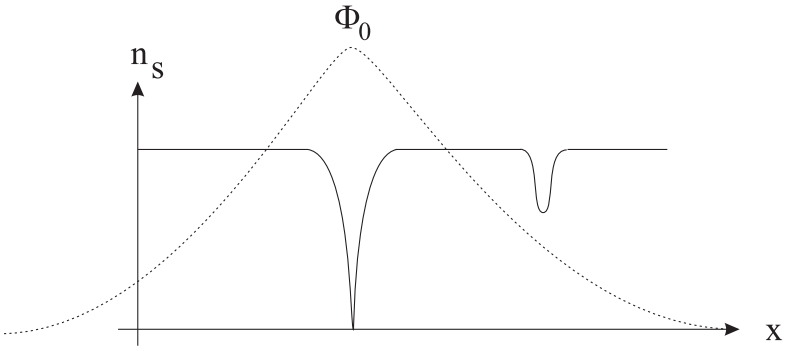

Figure 14. A flux line is shown on the left hand side with the Cooper pair density n_s going to zero at the core and a magnetic flux density indicated by the dash line. The superconducting state has a lower energy than the normal state whereby the system energy is increased by removing the Cooper pairs from the core of the flux line. If the flux line is created at a spot where the Cooper pair density is already low as shown on the right hand side of the figure fewer Cooper pairs have to be removed whereby the energy increase of the system is lower. Once the flux line is positioned at the weak spot it will stay there because the system energy will increase if it is moved. The weak spot therefore appear as an energy well and a force must be applied on the flux line in order to move it out of the well. The trapping of flux lines in weak spots is called pinning.

In section (5.2) it was argued that the critical current density was defined as the current resulting in a kinetic energy difference of the electrons in the Cooper pairs

exceeding the binding energy of the Cooper pairs. This is however not true for a type-II superconductor containing flux lines since the transport current density **J** will result in a force on the flux line acting perpendicular to both the flux line axis and the current direction. The force per unit length of flux line is [4]

$$\mathbf{f_t} = \mathbf{J} \times \mathbf{\Phi_0} \tag{37}$$

If the flux line move due to the applied force a work has been done on the system and energy has been lost. Thus a type-II superconductor in the mixed state can only carry a transport current without loss as long as the flux lines are pinned and the critical current density J_c is therefore determined by the de-pinning force $\mathbf{f_p}$ of the flux lines:

$$\mathbf{f_p} = \mathbf{J_c} \times \mathbf{\Phi_0} \tag{38}$$

Flux lines penetrating a type-II superconductor with pinning centers will be pushed from pinning center to pinning center and only move when the magnetic pressure from the applied field exceeds the pinning force. This result in a gradient of the flux line density, which is related to superconducting screening currents running at the edge of the superconductor by the Maxwell equation

$$\nabla \times \mathbf{B} = \mu_0 \mathbf{J} \tag{39}$$

Figure (15) show an example of magnetic flux penetration inside a superconductor containing pinning centers after the applied field has been increased to H_{app}. The magnetic flux density is plotted as function of the spatial position in the sample. At the sample edge the flux density is given by the applied field $B_z = \mu_0 H_{app}$, but it is decreasing towards the center due to the pinning of the flux lines and no magnetic field is present in the center part of the sample.

One can determine the circulating supercurrents at the edge from equation (39)

$$\mu_0 \mathbf{J} = \frac{\partial B_z}{\partial y}\widehat{x} - \frac{\partial B_z}{\partial x}\widehat{y} \tag{40}$$

which is illustrated on figure (15) by arrows labelled J_s . These supercurrents will cause a force acting perpendicular on both the flux line and the supercurrent direction as given by (37). Thus the screening supercurrents will push the flux lines into the center of the sample as shown on figure (15), but the flux lines will not move until the de-pinning force of the pinning centers is exceeded.

From the definition of the critical current density (38) and (40) it is seen that it can be related to a maximum gradient in the flux density

$$J_c = \left. \frac{1}{\mu_0} \frac{\partial B}{\partial x} \right|_{max} \tag{41}$$

Diamagnetism

The response of the superconductor to an applied field is to produce circulating screening supercurrents as shown on figure (15). One can imagine these currents as running in a coil generating a field with a direction opposite to and of a size equal to the applied field. A material with this property is called perfect diamagnetic, because the magnetization density of the sample balances the applied field giving $B = 0$ in the bulk.

[4] [9], chapter 5.4

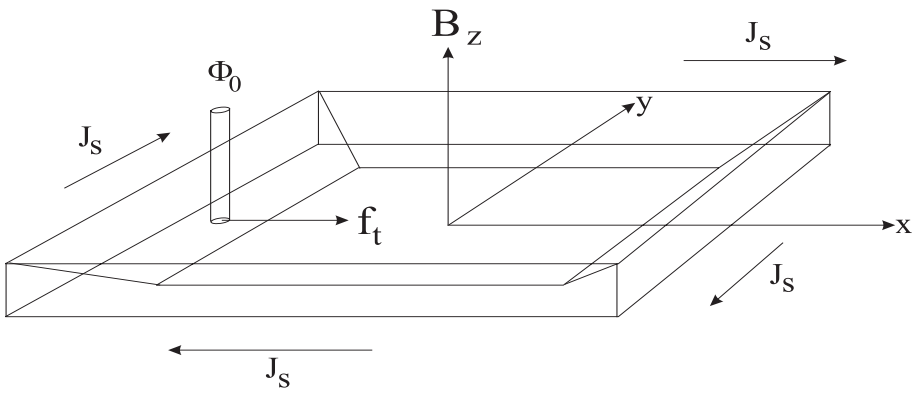

Figure 15. Plot of the spatial distribution of magnetic flux inside a pinning type-II superconductor after the applied field has been increased from zero. The magnetic flux density at the sample edge is given by the applied field $B_z = \mu_0 H_{app}$, but flux lines are prevented from entering the sample center due to the pinning. The magnetic field decreases from $\mu_0 H_{app}$ at the edge to $B_z = 0$ with a slope given by the critical current density. Arrows labelled J_s indicate the direction of the circulating supercurrents near the edges as found from Maxwells equation $\mu_0 \mathbf{J} = \nabla \times \mathbf{B}$. The circulating supercurrents give rise to a force $\mathbf{f_t} = \mathbf{J} \times \mathbf{\Phi_0}$ pushing the flux line Φ_0 into the center of the sample if the pushing force exceeds the pinning force of the pinning site.

$$\mathbf{B} = \mu_0(\mathbf{H} + \mathbf{M}) = 0 \Longrightarrow \mathbf{M} = -\mathbf{H} \tag{42}$$

The ability to screen out the applied field can be described by the susceptibility χ defined as $\mathbf{M} = \chi \mathbf{H}$. A susceptibility of $\chi = -1$ is obtained in the center part of the sample shown in figure (15) due to the flux exclusion and χ is increasing towards 0 as the edges are approached.

An evaluation of the levitation force of a superconductor in an external field can be determined from equation (25) in section (4.2) if the local magnetization given by

$$\mathbf{M} = \frac{\mathbf{B}}{\mu_0} - \mathbf{H} \tag{43}$$

can be calculated from a model describing the pinning properties of the superconductor. The simplest pinning model is known as the Bean model [12], in which the critical current density is assumed constant through out the sample. In this case the flux density will decrease linearly from the sample edge and with a slope given by the critical current density as shown on figure (15). More complicated models take into account a local dependence on the flux density.

5.5 Flux creep and flow

The thermal stability of the pinning of flux lines can be analyzed by considering a flux line Φ_0 pinned in a pinning potential well of size d and depth U_0 as shown on figure (16). A flux line can jump to a neighbor pinning site by a thermal activated process where the jump frequency f_j is given by

$$f_j = f_0 exp\left(-\frac{U}{k_B T}\right) \tag{44}$$

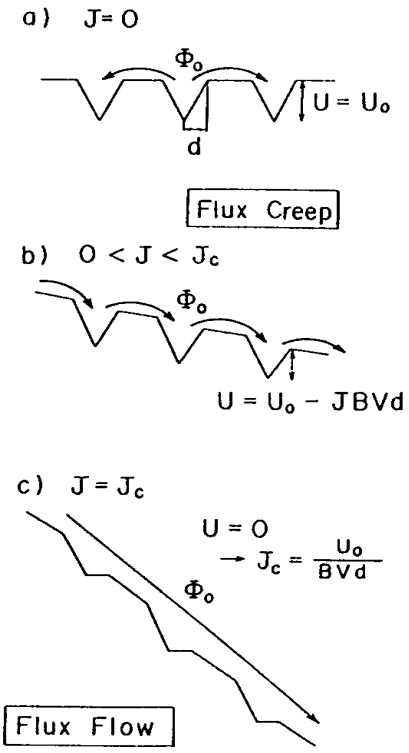

Figure 16. a) Thermal activated flux creep between pinning sites of size d and depth $U = U_0$. b) Enhanced flux creep from left to right caused by a transport current **J**. *c) Transition to flux flow regime when pinning sites become ineffective due to the transport current [13].*

where f_0 is the jump frequency when the thermal energy is much larger than the potential energy of the pinning site $k_BT >> U$.

A transport current or a flux gradient in the superconductor will increase the flux creep because of the interaction force per unit length $\mathbf{f_t} = \mathbf{J} \times \Phi_0$ (37) acting on the flux lines. A force is given by a gradient in the potential energy, which will have a constant slope in the case of transport currents or flux gradients

$$-\frac{dU}{dx} = f_t l = J\Phi_0 l \quad => \quad U(x) = U_0 - J\Phi_0 l x = U_0 - JBVx \tag{45}$$

where l is the length of the flux line, V the volume of the flux line $V = al$ and the flux quantum is given by the average magnetic flux density B and the flux line area a, $\Phi_0 = Ba$. Figure (16b) shows a linear changing potential energy caused by J. The pinning potential wells are changed since the left side of the well is increased by $\Delta U(-d) = U(-d) - U_0 = JBVd$ and the right hand side is lowered by $\Delta U(+d) = U(+d) - U_0 = -JBVd$ from equation (45). Thus the flux creep of flux lines from left to right is enhanced by the transport current. Figure (16c) shows the transition from the flux creep to the flux flow regime where the pinning centers are not effective any more. This gives a new definition of the critical current density J_c based on the physical properties of the pinning site

$$\Delta U(+d) = -J_c BVd = -U_0 \quad \Rightarrow \tag{46}$$

$$J_c = \frac{U_0}{BVd} = \frac{U_0}{\Phi_0 ld} \tag{47}$$

showing that one should increase the initial depth of the well per unit length of flux line $\frac{U_0}{l}$ or decrease the size of the well in order to increase the critical current density.

The above analysis shows that any non-uniform flux line distribution in a type-II superconductor will slowly decay towards a more uniform distribution by the flux creep mechanism if the temperature is sufficiently high or if large flux gradients are present.

5.6 History dependence

The state of a type-II superconductor containing pinning centers will not be reversible with the applied field because of the flux trapping at the pinning centers. This means that the levitation properties of the superconductor at a given temperature and field in the phase diagram shown on figure (13) will depend on the field and temperature history by which the superconducting state was entered from the normal phase. There are three fundamental different field and temperature histories

- Cooling below T_c in zero applied field and then increasing the field (zero field cooling).
- Cooling below T_c in a constant applied field (field cooling).
- Cooling to a given temperature in an applied field above H_{c2} and then decreasing the applied field below H_{c2}.

The zero field cooling procedure will cause the superconductor to enter the diamagnetic state where flux lines are prevented from moving into the bulk of the sample in the case of strong pinning. Flux lines will however slowly enter the superconductor due to the flux creep and the levitation force of the superconductor will thereby decrease slowly with time. Superconductors operated in this mode must occasionally be zero field cooled again in order to maintain a constant levitation force.

Field cooling creates a very homogeneous flux line distribution in the superconductor, because the magnetic field is gathered in flux lines at the pinning sites just below the critical temperature and will be pinned to these as the temperature is further decreased. If the external magnetic field is maintained constant then all flux lines will be in a stable equilibrium. The levitation force of a field cooled superconductor will be more stable than the zero field cooled superconductor, because the flux gradients will be smaller. This increased stability is often wanted in practical bearing applications.

A field decrease below the H_{c2} line (see figure (13)) at constant temperature will result in the creation of flux lines at pinning sites as the superconducting transition takes place. The flux lines will be maintained in the superconductor as the external field is decreased towards zero whereby large field gradients will result. In this way the superconductor will have properties equal to a permanent magnet, but the field strength of the superconducting permanent magnets can be several Tesla compared to 0.5 Tesla in the strongest conventional permanent magnets today. The flux line distribution obtained by this field decrease procedure will not be in equilibrium and change in time due to the flux creep process.

5.7 High temperature superconductors

From the discovery of superconductivity in 1911 until 1986 the highest critical temperature observed was $T_c = 23\ K$ for the type-II superconductor Nb_3Ge. This was in accordance with the upper limit of the Bardeen-Cooper-Schrieffer (BCS)

model, which provided a microscopic understanding of superconductivity in terms of the phonon-mediated interacting. The excitement was therefore large when a $T_c = 35\ K$ was reported in the $La_{2-x}Ba_xCuO_4$ ceramic material in 1986 [14]. Just one year later a $T_c = 93\ K$ was obtained in $YBa_2Cu_3O_{6+x}$ [15] and it was clear that these new superconductors could not be described by the BCS model. They were called "High Temperature (HTc) superconductors", because they violated the BCS theory in terms of critical temperature limit.

HTc superconductivity is still caused the creation of Cooper pairs, but of two holes and not two electrons. Until today there is still no microscopic understanding of the pairing mechanism, but it is clear that the BCS phonon-mediated interaction is not the answer. The highest reported $T_c = 133\ K$ is found in $Hg_{0.8}Pb_{0.2}Ba_2Ca_2Cu_3O_{8+\delta}$ [16].

All the HTc superconductors are of type-II and have upper critical fields H_{C2} in the range of several hundreds of Tesla, which in principle makes it possible to create very large magnetic fields with HTc superconductors. Also the possibility to obtain superconductivity upon cooling with liquid nitrogen, which boils at $T = 77\ K$, resulted in a reconsideration of the commercial use of superconductors, since the prize of liquid nitrogen is a factor of 100 smaller than liquid helium. One of the limiting factor of the use of HTc is to control the pinning of flux lines and to reduce the flux creep as outline above.

6 Superconducting bearings

Superconducting bearings are based on type-II superconductors ability to trap or expel external magnetic fields by pinning of flux lines in the bulk of the superconductor. Basic superconducting bearing design will be introduced and references to the literature are given in this chapter.

6.1 Basic designs

The most simple bearing configuration is similar to the demonstration experiment of the levitation of High Temperature (HTc) superconductors where a small permanent magnet is placed on top of the superconductor. Figure (17) shows three NdFeB magnets levitated above some $YBa_2Cu_3O_7$ pellets cooled with liquid nitrogen to $T = 77$ K. The magnets were placed on top of the superconductors after the cooling and the superconductors are therefore in the zero field cooled state where the magnetic field from the permanent magnets are expelled from the superconductors giving rise to the levitation force balancing gravity.

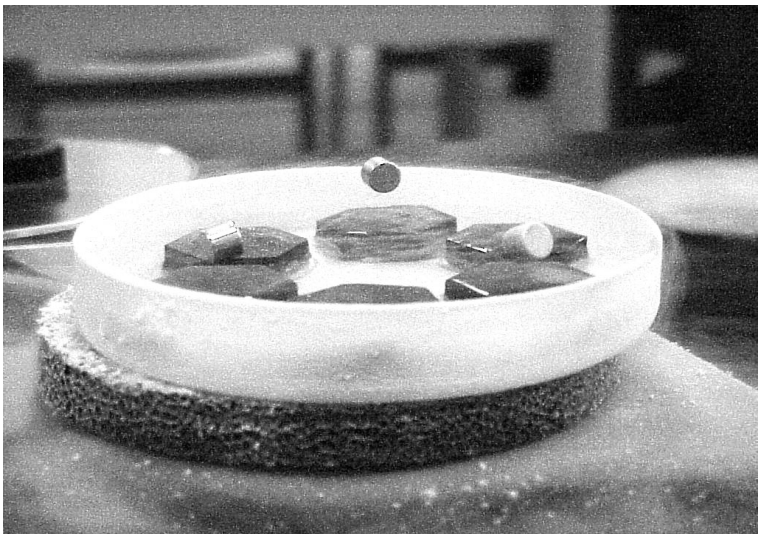

Figure 17. Levitation of permanent NdFeB magnets above $YBa_2Cu_3O_7$ HTc superconductor pellets cooled with liquid nitrogen.

A fundamental question is how Earnshaws theorem has been circumvented. If the external field from the magnet is expelled completely by the superconductor there will be no field component perpendicular to the superconductor surface. Such a field image is exactly what was found when two permanent magnets with equal poles were facing each other as shown on figure (5) in section (4). One can therefore consider the response of a superconductor to the field from a magnet as the creation of a field image of the magnet. This field image will rotate if the permanent magnet is rotated and the tilt instability found in section (4.1) has been removed by replacing the lower magnet in figure (2) by a superconductor. There is however no force preventing the permanent magnet from sliding sideways and eventually fall down at the edge of the superconductor.

The stabilization against sideways movement can be obtained if some of the field from the permanent magnet has penetrated the superconductor as flux lines which are trapped to pinning centers. Any movement of the permanent magnet giving rise to a change of the field will tend to redistribute the trapped flux lines

in the superconductor and a force will thereby act on the magnet.

The above analysis show that in order to levitate a rotating object one must construct the bearing such that the field from the magnet is not changed by the rotation. This is simply done by choosing the symmetry axis of the magnetic field as the rotation axis of the object.

6.2 Levitation force

The magnet-superconductor bearing shown on figure (18) is the simplest superconducting bearing consisting of a permanent magnet rotor and a superconductor underneath to levitate the rotor. The field symmetry axis of the permanent magnet is vertical as well as the rotation axis in order to obtain frictionless rotation.

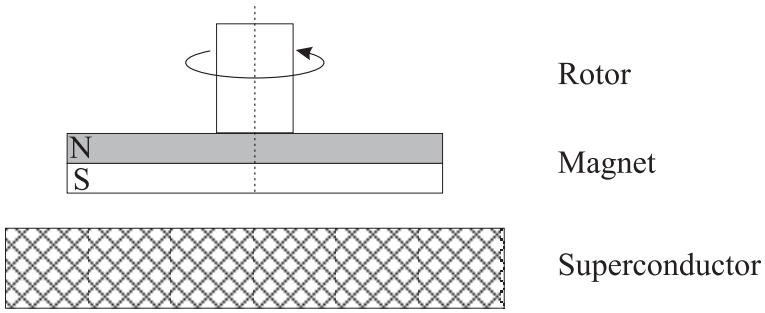

Figure 18. Simple superconducting bearing consisting of a permanent magnets and a superconductor underneath to provide the levitation force on the rotor.

Introductions to superconducting bearings can be found in [10, 4]

Zero field cooled bearing

One can estimate the levitation force of a zero field cooled magnetic-superconducting bearing by modeling the superconductor as the image of the magnet as explained in the introduction of this chapter and then evaluate the force between two magnetic dipoles.

The force between two magnetic dipoles of dipole moment m_1 and m_2 separated by a distance r between the centers of mass is given by [4]

$$F = -\frac{3\mu_0}{2\pi}\frac{m_1 m_2}{r^4} \tag{48}$$

Since the superconductor is considered as an image of the magnet and by assuming the magnetization density M of the magnet to be constant through out the sample one can set $m_1 = m_2 = MAL$. The area of the magnet has been denoted A and the length L, giving

$$F = -\frac{3\mu_0}{2\pi}\frac{M^2 A^2 L^2}{r^4} \tag{49}$$

The maximum levitation force per unit area can be evaluated by moving the dipoles so close together that they touch each other. This is equivalent to setting $r = L$. By further expressing the magnet area $A = \pi\frac{D^2}{4}$ from the diameter D one gets

$$\frac{F}{A} = -\frac{3}{8}\mu_0 M^2 \left(\frac{D}{L}\right)^2 = 8 \quad \mathrm{Ncm}^{-2} \tag{50}$$

where the magnetization density M of the strongest NdFeB magnets today $M = 4 \cdot 10^5$ $\mathrm{Am}^{-1}(\mathrm{B}_{\mathrm{surface}} = 0.5\ T)$ and a diameter to length ration of one have been inserted. This is a bit lower than the limit found from the magnetic pressure in section (4.3), because the geometry of the bearing has been included.

The above calculation is based on the assumption of complete flux exclusion, which depends on the flux pinning force and thereby the critical current density. In order to check the assumption one can evaluate the distance over which the screening of the field will take place from equation (41). By assuming the critical current density as constant one gets

$$\frac{\partial B}{\partial x} = \mu_0 J_c \Longrightarrow B(x) = B(0) - \mu_0 J_c x \tag{51}$$

By setting $B(x) = 0$ one can determine the field decay length l

$$l = \frac{B(0)}{\mu_0 J_c} \tag{52}$$

If this length l is small compared to the size of the sample one can assume that complete flux exclusion will be accomplished. Irradiated melt-textured $YBa_2Cu_3O_7$ [17] have $J_c = 5 \cdot 10^7$ Am^{-2} at $B = 0.5$ T whereby a field of $B(0) = 0.5$ T will be screened out in a distance of $l = 8.0$ mm which is quite large compared to many practical applications of bearings.

All the above is based on complete flux exclusion from the superconductor which therefore must be zero field cooled. This means that the magnet and rotor on figure (18) must be lifted away from the superconductor before the superconductor is cooled and then put back in operation position when the superconductor has entered the superconducting state. This operation complicates the construction of a practical superconducting bearing and most studies of superconductors are concerned with the levitation properties of field cooled superconductors were the magnet is kept in operation position during cooling.

Field cooled bearing

The evaluation of the levitation force of a field cooled superconductor is much more complicated than the flux exclusion calculation outlined in the previous section. A simple pinning model inspired by [18] will be introduced here to emphasize the basic physics of the levitation force of field cooled superconductors.

Figure (19) shows a field cooled superconductor in the air gab between two different magnetic poles. The magnetic field of the magnets is packed together in flux lines as the superconductor is cooled below the critical temperature as shown on the left hand side. It has been assumed that the superconductor is maintained in the same position during cooling by a mechanical support. The right hand figure shows what happens if the superconductor is displace by a distance Δx. It is only the part of the superconductor at the air gab edge which will be exposed to a different field resulting in forces tending to redistribute the flux lines. An upward directed force will be acting on the top flux line but the flux pinning will prevent it from moving resulting in an upwards directed levitation force on the superconductor. A similar upward directed force result from the bottom flux line.

By assuming that each flux line can support a force given by the maximum pinning force and that the total force is simply the sum of the pinning force on each flux line one can evaluate the force on the superconductor by integrating the pinning force density in the volume where the magnetic field is changed by the displacement of the superconductor. The maximum pinning force per unit length of a flux line is given by (38) and the pinning force density f_{pd} is found by

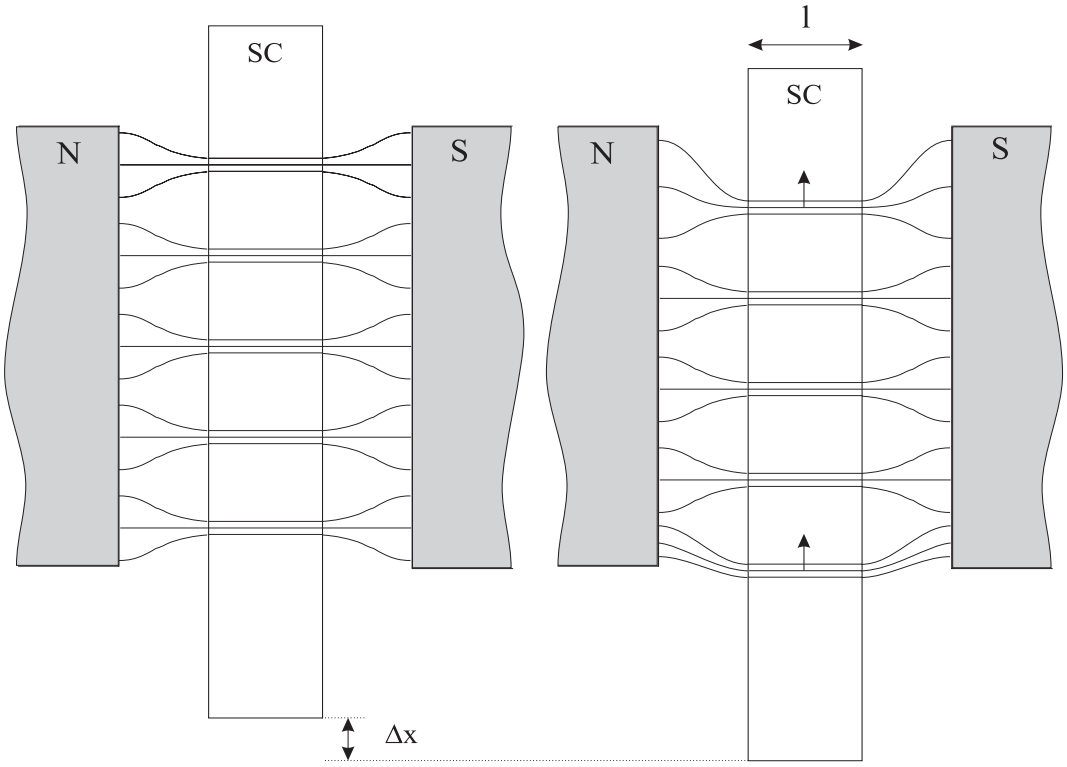

Figure 19. Left: Field cooled superconductor in the air gab between two permanent magnets. The magnetic flux in the superconductor is concentrated in flux lines as the superconducting state is entered. Right: Distortion of magnetic field due to the displacement of the superconductor in which the flux lines are pinned. An upward directed force will be acting on the top and bottom flux line, because the flux line density is respectively too low and high compared to the magnetic field at the edge of the air gab. The pinning of the flux lines prevents the flux lines from moving and an upward levitation force on the superconductor results. Flux lines in the center of the air gab are unaffected by the displacement of the superconductor, because the magnetic field is unchanged.

expressing the flux quantum from the average magnetic flux density B and the area A of the flux line $\Phi_0 = BA$

$$f_p = J_c\Phi_0 = J_cBA \Rightarrow f_{pd} = \frac{f_p}{A} = J_cB \tag{53}$$

The total force on the superconductor is then found by integrating the pinning force density in the volume V_f where the magnetic field is changed by the displacement.

$$F = -\int_{V_f} f_{pd}dV = -J_cBV_f \tag{54}$$

A constant pinning force density is assumed in the above. The volume where the field is changed will be proportional with the displacement Δx, the length of the flux lines l and size w of the superconductor perpendicular to the field and displacement whereby $V_f = lw\Delta x$. Thus

$$F = -J_cBlw\Delta x \tag{55}$$

By defining the area of the superconductor which is perpendicular to the force direction as the bearing area $A_B = lw$ one can evaluate the bearing force per bearing area and displacement using $J_c = 5 \cdot 10^7$ Am^{-2} and $B = 0.5$ T.

$$\frac{F}{A_B \Delta x} = J_c B = 2.5 \quad \text{Ncm}^{-2}\text{mm}^{-1} \tag{56}$$

The above model is extremely simplified because flux line interaction and depinning is not included. Flux lines will repel each other and the force on one flux line can thereby be coupled to the pinning of other flux lines in the neighborhood. This result in non-local force relations and the calculation of levitation forces includes solving a 3D pinning model giving the magnetic field distribution inside the superconductor whereby a force determination from (25) can be applied. Often the equation must be solved self consistent.

Literature

Many initial studies of superconducting bearings were made on small systems consisting of only a superconductor and a permanent magnet which was used as rotor [18, 19, 1, 20, 21, 22, 23]. An examination of the levitation force of a rotating bearing is difficult, because the force of gravity can not be changed continuously during an experiment. Most studies of the levitation force has therefore been carried out on stationary systems were the levitation force is measured by a balance holding the magnet. Figure (20) shows an example of such a static measurement setup [24]. Similar studies can be found in [25, 26, 27] where levitation forces on the same order of magnitude as estimated above was found.

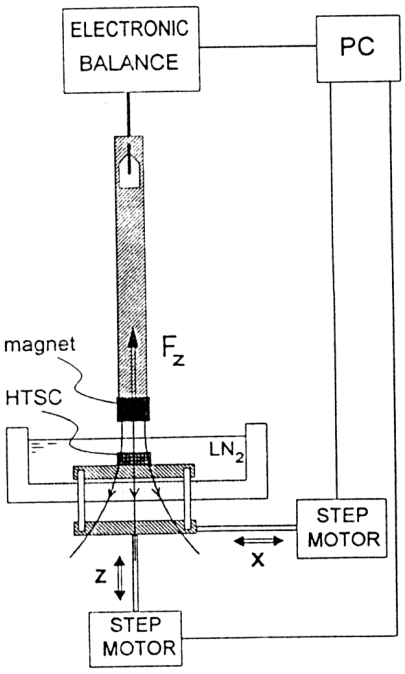

Figure 20. Setup for measuring the static displacement dependence on the levitation force between a permanent magnet mounted on a balance and a superconductor on a movable x-z stage [24]

Any improvement of the critical current density will increase the levitation force of the superconductor as seen from equation (56, 52). The development of

the processing of superconducting pellets is therefore crucial for the bearing applications. A group at Forschungszentrum Karlsruhe has obtained good results on the $YBa_2Cu_3O_7$ processing and obtained levitation forces of the order 18 Ncm^{-2} for a zero field cooled and 4.1 Ncm^{-2} for a field cooled superconductor using a $B = 0.45$ T permanent magnet of diameter $D = 25$ mm [28, 29]. Improvement of the superconductor levitation force by oxygenation of $YBa_2Cu_3O_x$ pellets for 10 hours at 450 °C has been reported in [30]. This improvement is caused by an increase of the oxygen contents x in the surface of the $YBa_2Cu_3O_x$ towards the optimum value at $x = 1$.

Many model studies of levitation force calculations for more sophisticated geometries and pinning description have been conducted. Size effects of superconductor and magnet are given in [31] and levitation forces of magnets placed on top of a superconducting ring is found in [32], both studies being based on a Meissner description of the superconductor. More full blown calculations are given in [33, 34, 35, 36] which are based on more complicated pinning models for describing the superconductor and finite element solution schemes for solving the system of equations self-consistently.

6.3 Stiffness

In the introductory discussion of this chapter it was noted that no restoring force preventing sideways movement of the magnet would be present in the case of complete flux expulsion. Pinning of flux lines however lead to a restoring force as described by equation (55) in the simple geometry of figure (19). The stiffness defined by equation (1) in this simple geometry is positive and given by

$$\kappa = J_c B l w \tag{57}$$

The order of the stiffness per bearing area is of the same size as found in equation (56).

An evaluation of the stiffness of the bearing geometry shown on figure (18) is more difficult because the field distribution is three dimensional. Figure (21) shows qualitatively how the distribution of magnetic field lines look before the cooling. The field distribution will result in curved flux lines in the superconductor with a similar geometry after the cooling into the superconducting state. All flux lines with a component in the horizontal plane will prevent the movement of the permanent magnet in the vertical direction due to the pinning of the flux lines. In the case of horizontal movement of the magnet all flux lines with a vertical component will prevent this. Thus the stiffness of the bearing will be positive in all three direction in contrast to the magnetic bearing where Earnshaws theorem applies.

Application of multipole magnets has been proposed to increase the stiffness of superconducting bearings. Figure (22) show such a design which will cause a redistribution of flux lines not only at the edges of the magnet, but also under the magnet in the case of horizontal displacements.

An alternative configuration to the magnet-superconductor bearing is to use a hybrid magnet-superconducting bearing. Figure (23) shows the hybrid bearing consisting of two magnets which supplies the levitation force of the bearing and a slab of superconductor in between the magnets is stabilizing the bearing by giving an overall positive stiffness in all three coordinates. The bearing stiffness can be adjusted by changing the amount of superconductor in between the magnets. One advantage of the hybrid bearing is that the levitation force is still present when the superconductor is warmed above the critical temperature. Thus the mechanical

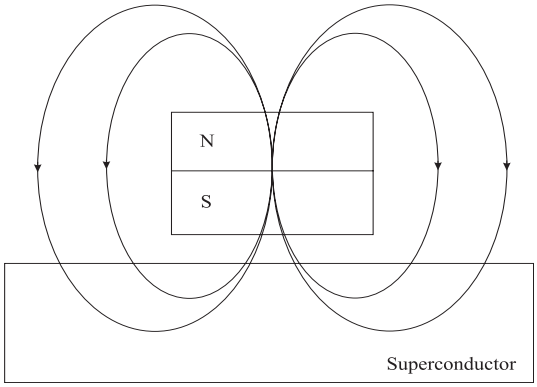

Figure 21. Distribution of magnetic field in a magnet superconductor bearing before the superconductor is field cooled. Flux lines with a similar geometry will be created as the superconductor is cooled below the superconducting transition temperature.

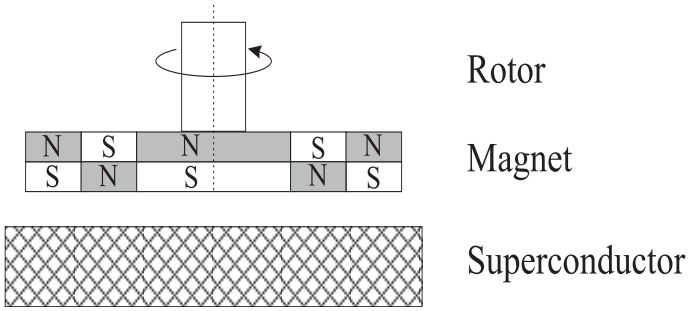

Figure 22. Magnetic-superconducting bearing constructed of a multipole magnet in order to increase the stiffness of the bearing.

support for the rotor in non rotating modes only needs to keep the rotor in position and not to support the whole mass of the rotor.

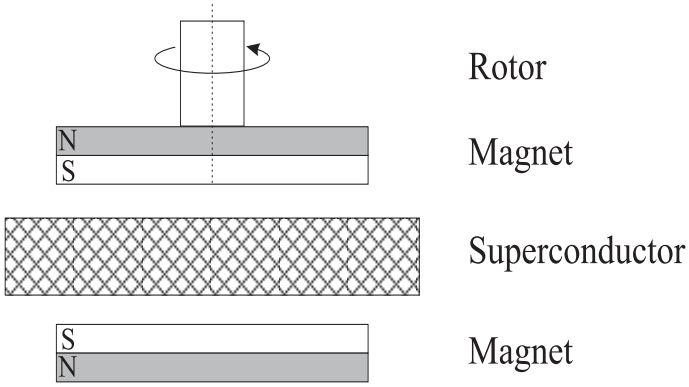

Figure 23. Hybrid magnetic-superconducting bearing where the levitation force is created by the repulsion of two permanent magnets and the stabilization is obtained by the flux pinning in the slab of superconductor in between the magnets.

Literature

A number of studies of the superconductor bearing stiffness has been conducted on setups similar to figure (20). A stiffness of the order 10^{-3} - 10^{-1} Nmm^{-1} and 10^{-2} - $5 \cdot 10^{-1}$ Nmm^{-1} was found for vertical and horizontal displacement respectively in granular superconductors [24]. A good agreement between model and experiments was obtained by describing the grains of the superconductor by the Bean pinning model. Similar results have been reported in [26, 21].

An increase of the bearing stiffness by a factor of 5 when using the multipole bearing configuration has been reported for a 300 g flywheel [22]. Studies of hybrid bearings can be found in [18, 20, 37, 38, 39].

A high stiffness of $YBa_2Cu_3O_7$ thin films of a thickness of 0.3 μm have been reported in [40]. It has been suggested that such films are used as stabilizing elements in space application where gravity is no problem.

6.4 Coefficient of friction

Figure (24) show a typically flywheel bearing loss experiment where a permanent magnet rotor is levitated above some HTc superconductors cooled by liquid nitrogen [1]. The positioning device on the right hand side is used to place the superconductor in operation position before the superconductor is field cooled. Levitation heights between 3 and 9 mm were obtained for a the 320 gram rotor by removing the positioning stick after cooling of the superconductor. A jet of nitrogen gas was injected into the vacuum chamber through the tube at left to spin up the rotor. By measuring the decrease of the rotation speed as function of time the authors could determine the bearing losses and calculate the coefficient of friction from equation (5).

The three main contribution to the losses in superconducting bearings are

- Viscous drag forces caused by the residual gas in the vacuum chamber.
- Heat generation in conducting parts in the neighborhood of the rotating magnet caused by induction of eddy currents.
- Work done by moving pinned flux lines in the superconductor.

The mechanical drag force from the residual gas in the vacuum chamber is by far the largest loss mechanism and must be reduced by maintaining pressures in the test chamber below 10^{-4} mbar in order to study the intrinsic loss mechanisms in superconductor bearings.

Eddy currents are induced in rotating conducting materials if the magnetic field in the conductor is changing in time. From Maxwells equations one can calculate the induced electric potential U due to a time varying magnetic field in an area of a conductor :

$$\nabla \times \mathbf{E} = -\frac{\partial \mathbf{B}}{\partial t} \tag{58}$$

$$\int_{area} \nabla \times \mathbf{E} d\mathbf{S} = -\int_{area} \frac{\partial \mathbf{B}}{\partial t} d\mathbf{S} \tag{59}$$

$$U = \int_{loop} \mathbf{E} d\mathbf{l} = -\frac{\partial \Phi}{\partial t} \tag{60}$$

If the above is calculated for a magnet with a pole radius of r moving with a speed of v along the surface of a conducting plate one gets :

$$U = -\frac{B\pi R^2}{\frac{2r}{v}} = \frac{\pi B r v}{2} \tag{61}$$

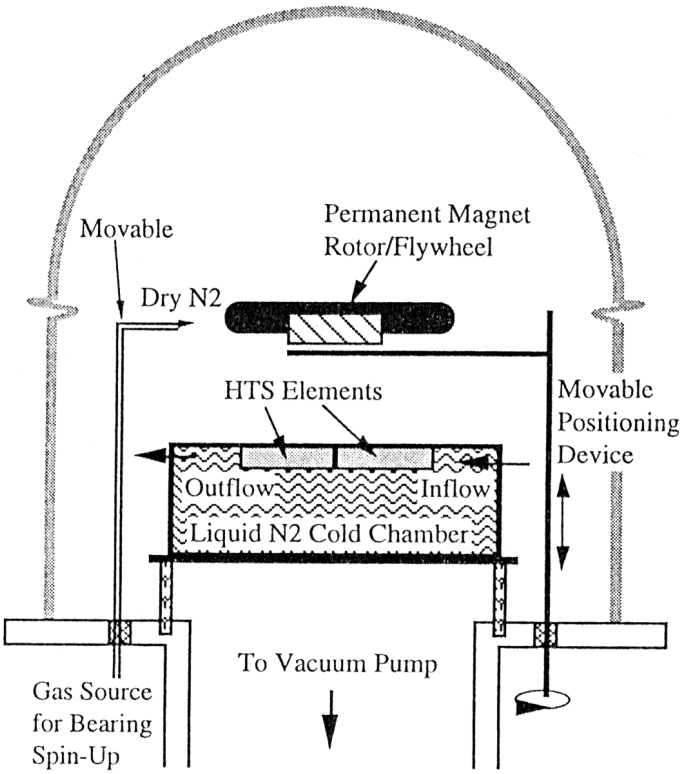

Figure 24. Experimental setup for loss determination in magnetic superconductor bearing. The magnet rotor is fixed above the superconductor with the positioning device shown on the right hand side while the superconductor is cooled below the critical temperature. Once the superconductor is cold the positioning device is removed and a jet of nitrogen gas introduced by the tube shown on the left hand side is used to initially spin up the rotor. Losses are then evaluated by measuring the decrease of the rotation speed as function of time. A coefficient of friction of 10^{-6} *was obtained with the shown setup [1].*

The losses can then be calculated from Ohm's law :

$$P = RU^2 = \frac{RB^2r^2v^2}{4} \tag{62}$$

where R is the resistance of the conductor along the circumference of the magnetic pole. If the conducting plate is rotating then the velocity v will be proportional with the angular velocity ω of the plate, $v = R_{plate} \cdot \omega$.

The above calculation shows that the volume of the parts in the bearing made from conducting material should be as small as possible.

When ever a pinned flux line is moved between pinning sites a work is done on the system and an energy loss result. It was previously shown that redistribution of the flux lines in the superconductor only occur when the magnet is displaced and it is thereby concluded that any asymmetry of the magnetic field from the permanent magnet will cause losses in the superconductor. A similar loss result if the mechanical rotation axis of the magnet is displaced with respect to the symmetry axis of the magnetic field or if mechanical vibrations in the bearing makes the position of the magnet oscillate.

The loss mechanisms mentioned above will all give rise to a constant energy loss per rotation of the permanent magnet whereby the loss will increase linear with

the rotation speed. A time constant is however connected to flux creep which will result in changes in the loss mechanisms as function of the rotation speed. This subject of loss mechanisms in superconducting bearings is still being investigated.

Literature

Coefficients of friction of the order 10^{-6} at rim velocities of $v_r = R\omega = 17$ ms^{-1} was obtained with a $R = 89$ mm diameter bearing shown on figure (24) [1]. A decrease by a factor of two was obtained by replacing the stainless steel of the liquid nitrogen cryochamber by a fiberglass/epoxy composite whereby eddy current losses were reduced.

Optimization of materials parameters and bearing geometry with respect to losses can be found in [20, 37, 41].

Hysteresis losses in superconductors have been described using the Bean model [42] and it has been shown that the hysteresis losses are proportional to the rotation speed where as the eddy current losses are proportional with the rotation speed squared [43].

A standard measurement method for characterization of superconductors is to measure the magnetic response of the superconductor when it is exposed to an alternating magnetic field. This method is called a.c. susceptibility and the losses determined in such a measurement are similar to the losses seen when the magnet rotor is causing a changing magnetic field. Several studies of relation between the two ways of probing losses have been performed [44, 45, 13]. It was found that grain boundaries in the superconductor resulted in high losses due to the weak pinning of the flux lines trapped in the grain boundary.

Reduction of the losses caused by an inhomogeneous magnetic field has been accomplished by gluing small sheets of ferro-magnetic material on permanent magnet rotors in order to remove the field inhomogeneity [46].

6.5 Dynamic stability

The purpose of a dynamic stability analysis is to determine if the motion of the bearing is stable with respect to tilts and changes of equilibrium position when the rotor is spinning. This can be determined by solving the equations of motion including magnetic forces and damping caused by the superconductor or induced eddy currents. The relation between magnetic force and displacement will often be non-linear as found in equation (49) and contain couplings between different directions. Thus the motion of a superconducting bearing must be described by non-linear coupled differential equations resulting in complicated dynamics such as chaotic solutions.

Analytical solutions to the non-linear coupled differential equation can very seldom be found and numerical solving or perturbation stability analysis in the neighborhood of steady-state solutions must often be applied to the systems.

Litterature

Perturbation theory has been applied to the equations of motion of a simple rotating bearing and it has been shown to have a divergent instability at certain critical rotation speeds [47, 48]. Such instabilities have been observed experimentally where external mechanical vibrations and internal mechanical resonances causes changes of the equilibrium position of the magnet in rotating bearings in respectively [49] and [50].

6.6 Large scale applications

This section will outline examples of large scale applications of superconducting bearings in flywheel systems. The following groups are the most active in the field:

- The Interdisciplinary Research Centre in Superconductivity (IRC) originating from the University of Cambridge. Key persons in flywheel research are A. M. Campbell and T. A. Coombs.
- Forschungzentrum Karlsruhe GmbH, Germany. Key persons are H.J. Bornemann and M. Sander.
- The Energy Technology Division at Argonne National Laboratory, USA. Key person is J. R. Hull.

The IRC group have constructed a flywheel system with a 43 kg rotor supported by magnetic-superconductor hybrid bearings. Figure (25) show the test setup where the levitation force on the composite glass/carbon fiber ring is provided by two magnets placed on the rotor shaft. The stability of the rotor is obtained by placing magnets on the rotor rim and superconductors underneath. Motors for spinning up the rotor and performing loss examinations are placed at the top of the setup [38]. Coefficients of friction of the system has been reduced to 10^{-6} by evacuating the test chamber to 10^{-6} mbar with a turbo pump [51]. The aim of the group is to build a 5 kWh flywheel system with a 5 kW energy conversion.

The group in Karlsruhe demonstrated coefficients of friction of 10^{-5} in a magnetic-superconducting bearing with a rotor of 3 kg spinning up to 15000 RPM. The maximum energy capacity was 4.8 Wh and maximum power was 1.5 kW [52]. They have later improved the design and obtained a 300 Wh / 10 kW system with a 10 kg rotor mass operating at 50000 RPM and superconductors at 77 K [53]. Figure (26) show the construction of the flywheel where a motor/generator is placed in the center of the shaft. A rotor and a superconducting bearing is placed on both sides of the motor. Figure (27) show a detailed drawing of the superconductor bearing construction which is cooled by a close cycle cryo cooler placed in the wall of the vacuum chamber. A coefficient of friction of 10^{-6} was obtained with the setup. The Karlsruhe group have worked out a design proposal for a 5 MWh/ 100 MW power plant based on superconducting flywheel technology [53].

The Argonne group have mostly been active in the basic research of loss mechanisms in the superconducting bearings, but they have recently initiated large scale test of flywheels with masses between 10-100 kg as announced on their home page and in [54].

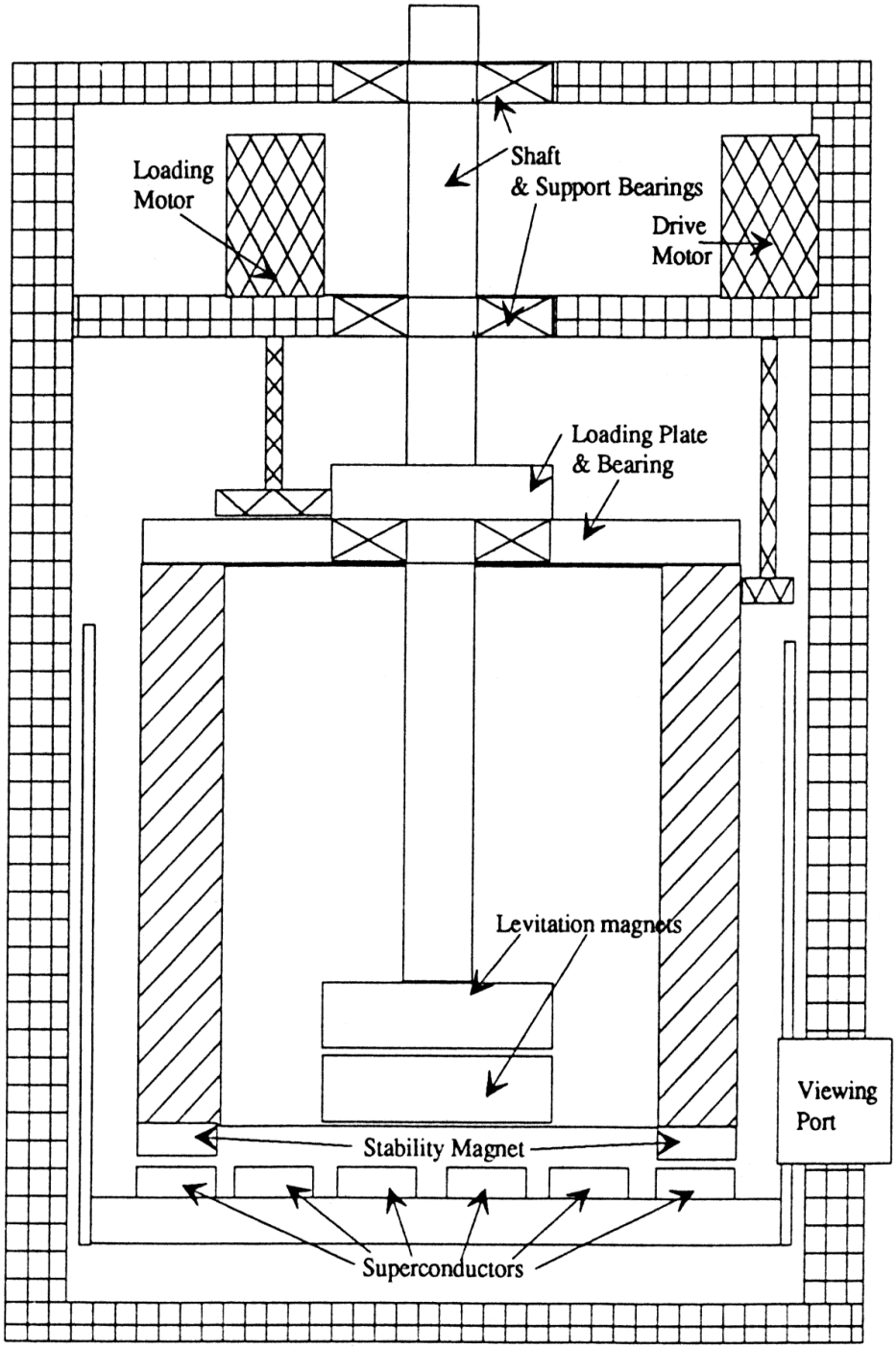

Figure 25. 43 kg flywheel supported by a hybrid-superconducting bearing [38].

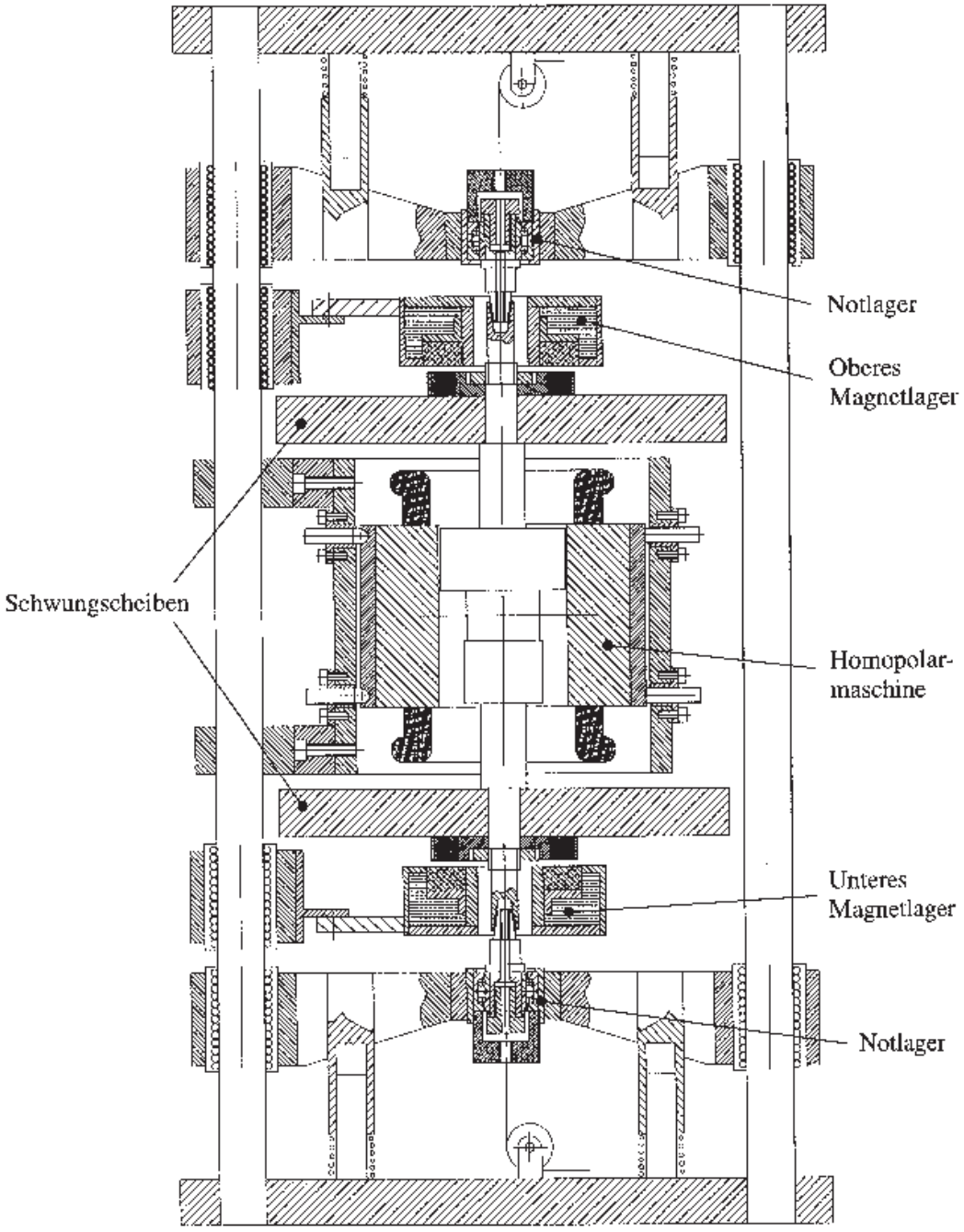

Bild A.3: Konstruktionsskizze des Schwungradspeicher-Prototyps

Figure 26. 300 Wh/10 kW flywheel with a 10 kg rotor spinning at 50000 RPM. A combined flywheel/motor/generator is placed in the center and the superconducting bearings are seen at the top and bottom.

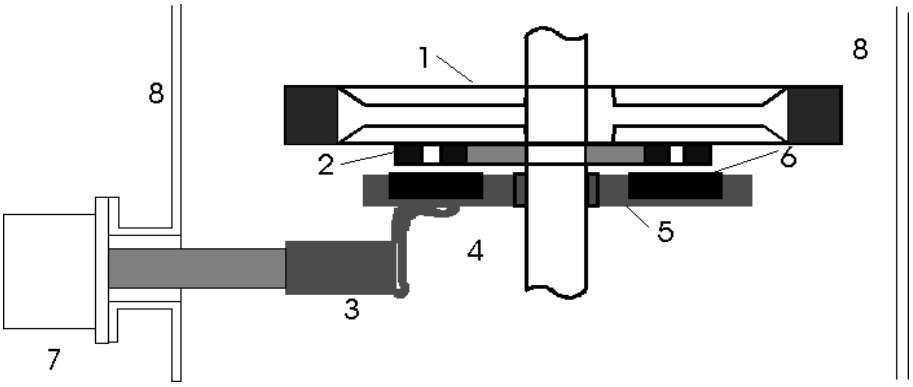

Figure 27. Construction of superconducting bearing of the Karlsruhe group. 1: Flywheel disc. 2: Permanent magnet. 3: Coldhead. 4: Flexible copper lead. 5: Cold plate. 6: Superconducting ring. 7: Cryocooler. 8: Vacuum chamber.

7 Conclusion

This report has examined the basic properties of superconducting bearings and the following can be concluded

- Levitation forces of the order 10 Ncm^{-2} can be obtained for zero field cooled superconductors and for hybrid magnetic superconducting bearings. Field cooled superconductors can provide levitation forces of the order 1 Ncm^{-2}. Sufficient levitation force for supporting a 20 kg flywheel is thereby obtainable.
- The stiffness of superconducting bearings is of the order 1 $\mathrm{Ncm}^{-2}\mathrm{mm}^{-1}$. This is enough for stabilizing flywheels operating in stationary applications.
- A reduction of the coefficient of friction can be improved by 3 orders of magnitude when conventional bearings are replaced by superconducting bearings. Practical flywheel applications have demonstrated coefficients of friction as low as 10^{-6}.
- The dynamics of superconducting bearings is much more complicated than conventional bearings, because of non-linear force-displacement relation. Thus stability analysis of specific flywheel systems is very important in the design of practical superconducting flywheel applications.

Superconducting flywheels with properties similar to the Risøflywheel have already been constructed and been proven to function by several research groups.

References

[1] J.R. Hull, T.M. Mulcahy, K.L. Uherka, and R.G. Abboud. Low rotational drag in High-temperature superconducting bearing. *IEEE trans. superconductivity*, 5:626–629, 1995.

[2] S. Earnshaw. On the nature of the molecular forces which regulate the constitution of the luminiferous ether. *Trans. Camb. Phil. Soc.*, 7:97–112, 1842.

[3] B.I. Bleaney and B. Bleaney. *Electricity and Magnetism.* Oxford University Press, 1991.

[4] F.C. Moon. *Superconducting Levitation.* John Wiley and Sons Inc., 1994.

[5] D. J. Jackson. *Classical Electrodynamics.* John Wiley and Sons Inc., 1962.

[6] Vacuumschelze commercial 1997. Rare-Earth Permanent Magnets VACODYM VACOMAX.

[7] C.J. Gorter and H.B.G. Casimir. *Phys. Z.*, 35:963, 1934.

[8] C.J. Gorter and H.B.G. Casimir. *Physica*, 1:306, 1934.

[9] M. Tinkham. *Introduction to superconductivity.* McGraw-Hill, Inc., 1996.

[10] B. Seeber. *Handbook of applied superconductivity.* Institute of physics publishing, 1998. Chapter G9 by T.A. Coombs on superconducting magnetic bearings.

[11] A.B. Abrahamsen. *Bitter decoration of the flux line lattice in Type-II superconductors.* Master thesis, Risø National Laboratory, Condensed Matter Physics and Chemistry Department, 1998.

[12] C.P. Bean. Magnetization of hard superconductors. *Phys. Rev. Lett.*, 8(6):250–253, 1962.

[13] M. Uesaka, A. Suzuki, N. Takeda, Y. Yoshida, and K. Miya. A.c. magnetic properties of YBaCuO bulk superconductor in high tc superconducting levitation. *Cryogenics*, 35:243–247, 1995.

[14] J.G. Bednorz and K.A. Muller. *Z. Phys. B - Condensed Matter*, 64:189, 1986.

[15] M.K. Wu, J.R. Ashburn, and C.J. Torng. *Phys. Rev. Lett.*, 58:908, 1987.

[16] A. Schilling, M. Cantoni, J.D. Guo, and H.R. Ott. *Nature*, 363:56, 1993.

[17] J.K.S. Christiansen, N.H. Andersen, and T. Frello. Pinning of magnetic flux lines in $Y-Ba-Cu-O$ superconductors by neutron irradiation and chemical route. *IEEE trans. superconductivity*, 9:2304–2307, 1999.

[18] K.B. Ma, C.K. McMichael, M.A. Lamb, and W.K. Chu. Application og high temperature superconductors on levitation bearings, torque transmissions and vibration dampers. *IEEE trans. superconductivity*, 3(1):388–391, 1993.

[19] J.R. Hull, J.L. Passmore, T.M. Mulcahy, and T.D. Rossing. Stable levitation of steel rotors using permanent magnets and high-temperature superconductors. *J. Appl. Phys.*, 76(1):577–580, 1994.

[20] J.R. Hull, E.F. Hilton, T. M. Mulcahy, Z.J. Yang, and A. Lockwood. Low friction in mixed-mu superconducting bearings. *J. Appl. Phys.*, 78(11):6833–6838, 1995.

[21] S. Nagaya, N. Hirano, M. Takenaka, M. Minami, and H. Kawashima. Fundamental study on high-tc superconducting magnetic bearings for flywheel system. *IEEE trans. superconductivity*, 5(2):643–649, 1995.

[22] M. Komori, A. Tsuruta, S. Fukata, and T. Matsushita. Superconducting bearing system using high tc superconductors. *IEEE trans. superconductivity*, 5(2):634–637, 1995.

[23] C. E. Rossman and J. I. Budnick. Precession of spinning magnets levitated over high-temperature superconductors. *Physica C*, 295:304–329, 1998.

[24] T. H. Johansen, H. Bratsberg, A.B. Riise, H. Mestl, and A.T. Skjeltorp. Measurements and model calculations of forces between a magnet and granular high-tc superconductor. *Applied Superconductivity*, 2(7/8):535–548, 1994.

[25] P. Tixador, P. Hiebel, Y.Brunet, X. Chaud, and P. Grautier-Picard. Hybrid superconducting magnetic suspensions. *IEEE trans. magnetics*, 32(4):2578–2581, 1996.

[26] H. Ishigaki, H. Ito, M. Itoh, A. Hida, and R. Takahata. Magnetic coupling by using levitation characteristics of YBCO superconductors. *IEEE trans. superconductivity*, 3(1):404–407, 1993.

[27] E. H. Brandt. Friction in levitated superconductors. *Appl. Phys. Lett.*, 53(16):1554–1556, 1988.

[28] A.W. Kaiser, M. Adam, and H.J. Bornemann. Characterization and properties of batch-processed melt-textured YBCO. *Supercond. Sci. Technol.*, 11:26–29, 1998.

[29] H.J. Bornemann, T. Burghardt, W. Hennig, and A. Kaiser. Processing technique for fabrication of advanced YBCO bulk materials for industrial applications. *IEEE trans. superconductivity*, 7(2):1805–1808, 1997.

[30] D. Shi, D. Qu, and B.A. Tent. Effects of oxygenation on levitation force in seeded melt grown single-domain $YBa_2Cu_3O_x$. *Physica C*, 291:181–187, 1997.

[31] S. Sagar, K. Lahiri, and D. Shi. Effect of sample geometry on levitation force in seeded-melt-grown single-domain $YBa_2Cu_3O_x$. *IEEE trans. superconductivity*, 7(2):1929–1932, 1997.

[32] Z.J. Yang. Levitation forces acting on a magnet placed over a superconducting ring. *Applied Superconductivity*, 2(7/8):559–569, 1994.

[33] M. Tsuchimoto and T. Honma. Numerical evaluation of levitation force of HTSC flywheel. *IEEE trans. superconductivity*, 4(4):211–215, 1994.

[34] A.O. Hauser. Calculation of superconducting magnetic bearings using commercial FE-program (ANSYS). *IEEE trans. magnetics*, 33(2):1572–1575, 1997.

[35] T.A. Coombs, D.A. Cardwell, and A. M. Campbell. Dynamic properties of superconducting magnetic bearings. *IEEE trans. superconductivity*, 7(2):924–927, 1997.

[36] I. Vajda and L. Mohcsi. Advanced hysteresis model for levitating applications of HTSC materials. *IEEE trans. superconductivity*, 7(2):916–919, 1997.

[37] J. R. Hull, T. M. Mulcahy, and J.F. Labataille. Velocity dependence of rotational loss in evershed-type superconducting bearings. *Appl. Phys. Lett.*, 70(3):655–657, 1997.

[38] T.A. Coombs, A.M. Campbell, I. Ganney, W. Lo, T. Twardowski, and B. Dawson. Superconducting bearings in flywheels. *Materials science and Engineerings B*, 53:225–228, 1998.

[39] Z. Xia, Q.Y. Chen, K.B. Ma, C.K. McMichael, M. Lamb, R.S. Cooley, P.C. Fowler, and W.K. Chu. Design of superconducting magnetic bearings with high levitating force for flywheel energy storage systems. *IEEE trans. superconductivity*, 5(2):622–625, 1995.

[40] P. Schonhuber and F.C. Moon. Levitation forces, stiffness and force-creep in YBCO high-tc superconducting thin films. *Applied Superconductivity*, 2(7/8):523–534, 1994.

[41] C. Navau and A. Sanchez. Stability and losses of levitating superconducting disk and cylinders. *IEEE trans. superconductivity*, 7(2):920–923, 1997.

[42] W.C. Chan, D.S. Jwo, and J.J. Lee. Bean's model and magnetic flux-drag torque for high-tc superconductors. *Physica C*, 252:203–207, 1995.

[43] M. Zeisberger and W. Gawalek. Losses in magnetic bearings. *Mat. Scin. Engineering B*, 53:193–197, 1998.

[44] C. E. Rossman, J. I. Budnick, and B. R. Weinberger. Correlation of frictional losses of spinning levitated magnets with ac susceptibility in high-temperature superconductors. *Appl. Phys. Lett.*, 70(2):255–257, 1997.

[45] Z. J. Yang and J. R. Hull. Energy loss in superconducting bearing systems. *IEEE trans. superconductivity*, 7(2):318–321, 1997.

[46] J. R. Hull, J.F. Labataille, T. M. Mulcahy, and J.A. Lockwood. Reduced hysteresis loss in superconducting bearings. *Appl. Supercond.*, 4(1/2):1–10, 1996.

[47] T. Sugiura, Y. Uematsu, and T. Aoyagi. Dynamics of a rotor levitated above a high-tc superconductor. *Inst. Phys. Conf. Ser.*, (158):1523–1526, 1997.

[48] T. Sugiura, M. Tashiro, Y. Uematsu, and M. Yoshizawa. Mechanical stability of a high-tc superconducting levitation system. *IEEE trans. superconductivity*, 7(2):386–389, 1997.

[49] T. Hikihara, H. Adachi, S. Ohashi, Y. Hirane, and Y. Ueda. Levitation drift of flywheel and HTSC bearing system caused by mechanical resonance. *Physica C*, 291:34–40, 1997.

[50] T. A. Coombs and A. M. Campbell. Gap decay in superconducting magnetic bearings under the influence of vibration. *Physica C*, 256:298–302, 1996.

[51] T. Coombs, A.M. Campbell, R. Storey, and R. Weller. Superconducting magnetic bearings for energy storage flywheels. *IEEE trans. superconductivity*, 9(2):968–971, 1999.

[52] H.J. Bornemann, A. Tonoli, T. Ritter, C. Urban, O. Zaitsev, K. Weber, and H. Rietschel. Engineering prototype of a superconducting flywheel for long term energy storage. *IEEE trans. superconductivity*, 5(2):618–621, 1995.

[53] H.J. Bornemann and M. Sander. Conceptual system design of a 5 MWh/100 MW superconducting flywheel energy storage plant for power utility applications. *IEEE trans. superconductivity*, 7(2):398–401, 1997.

[54] T.M. Mulcahy, J.R. Hull, K.L. Uherka, R.C. Niemann, R.G. Abboud, J.R. Juna, and J.A. Lockwood. Flywheel energy storage advances using HTS bearings. *IEEE trans. superconductivity*, 9(2):297–301, 1999.

Bibliographic Data Sheet **Risø–R–1265(EN)**

Title and author(s)

Superconducting bearings for flywheel applications

Asger Bech Abrahamsen

ISBN	ISSN
87–550–2877–2(internet)	0106–2840

Dept. or group	Date
Materials Research Department	2/5-2001

Groups own reg. number(s)	Project/contract No.

Pages	Tables	Illustrations	References
45	0	27	54

Abstract (Max. 2000 char.)

A literature study on the application of superconducting bearings in energy storage flywheel systems. The physics of magnetic levitation and superconductors are presented in the first parts of the report, followed by a discussion of the literature found on the applications of superconducting bearings in flywheels.

Descriptors INIS/EDB

FLYWHEELS; HIGH-TC SUPERCONDUCTORS; MAGNETIC BEARINGS; REVIEWS